

University of Alberta

Aggregate Interference Analysis for Cognitive Radio Networks

by

Sachitha Panduka Kusaladharma

A thesis submitted to the Faculty of Graduate Studies and Research
in partial fulfillment of the requirements for the degree of

Master of Science

in

Communications

Electrical and Computer Engineering

©Sachitha Panduka Kusaladharma

Fall 2013

Edmonton, Alberta

Permission is hereby granted to the University of Alberta Libraries to reproduce single copies of this thesis and to lend or sell such copies for private, scholarly or scientific research purposes only. Where the thesis is converted to, or otherwise made available in digital form, the University of Alberta will advise potential users of the thesis of these terms.

The author reserves all other publication and other rights in association with the copyright in the thesis and, except as herein before provided, neither the thesis nor any substantial portion thereof may be printed or otherwise reproduced in any material form whatsoever without the author's prior written permission.

Dedicated to my beloved parents...

Abstract

In underlay Cognitive Radio (CR) systems, secondary users may transmit while primary transmissions take place. However, the interference aggregates on the primary system, and performance degradation will occur. Thus, quantifying and modeling of the aggregate interference is important in characterizing the network's performance. An interference analysis for a Poisson process of CR nodes in a finite area is undertaken while incorporating channel parameters, and a simple Gamma model for the aggregate interference is proposed. Furthermore, a multiple-ring model to replace the annular underlay model will be developed. This model is versatile and mathematically tractable, while being highly accurate. Moreover, the interference from the nearest interferer node is analyzed, and situations where the nearest interferer's interference can approximate the aggregate interference are identified. An outage and asymptotic analysis is carried out for the models. The effect of different system and channel parameters are shown within the numerical results.

~

Acknowledgements

I would like to thank Dr Chintha Tellambura for being an excellent supervisor and guiding me on my path of research. I also wish to thank all my family and friends and other teachers who have helped me to come to this stage.

~

Contents

1	Introduction	1
1.1	Wireless Communications	1
1.2	Methods to improve spectral efficiency	2
1.2.1	Cognitive radio	2
1.2.2	Heterogeneous networks	5
1.2.3	Small cell networks	5
1.3	Problem Statement	6
1.4	Contributions and Outline	6
2	Background	9
2.1	The wireless channel	9
2.1.1	Multipath fading and the Doppler effect	9
2.1.2	Small scale fading models	11
2.1.3	Shadowing	12
2.1.4	Path loss	14
2.1.5	Power control	15
2.2	Spatial distribution models	15
2.2.1	Poisson point process	16
2.2.2	Binomial point process	17
2.3	Annular underlay networks	18
2.3.1	Aggregate interference	20
2.4	Conclusion	21
3	Aggregate Interference Analysis	22

3.1	Introduction	22
3.2	Aggregate interference of annular underlay networks	23
3.2.1	Introduction	23
3.2.2	System model	23
3.2.3	Interference Statistics	24
3.2.4	Performance Analysis	26
3.3	Gamma model approximation	28
3.3.1	Introduction	28
3.3.2	The Gamma Approximation	29
3.4	Numerical Results	30
3.4.1	Numerical results of Aggregate interference for annular underlay networks	30
3.4.2	Numerical results for the Gamma approximation	35
3.5	Conclusion	37
4	Approximation models for the aggregate interference	40
4.1	Introduction	40
4.2	A multiple-ring model for underlay interference	41
4.2.1	Introduction	41
4.2.2	Proposed System Model	42
4.2.3	Interference Statistics	43
4.2.4	Suitability as a stand-alone system model	47
4.2.5	Performance analysis	49
4.3	Nearest Interferer approximation	55
4.3.1	Introduction	55
4.3.2	System model	56
4.3.3	Distribution of the nearest interferer node	57
4.3.4	Derivation of the MGF	60
4.3.5	Moments	63
4.3.6	Outage Analysis	64
4.4	Numerical Results	65

4.4.1	Numerical results of the multiple-ring model	65
4.4.2	Numerical results for the nearest interferer approximation .	68
4.5	Conclusion	71
5	Conclusions and Future Research Directions	74
5.1	Conclusions	74
5.2	Future Research Directions	75
	Bibliography	77

List of Tables

- 4.1 Error statistics for $R = 5$ and $M = 20$ 54
- 4.2 Error statistics for $R = 1$ and $M = 100$ 54

List of Figures

1.1	Spectral efficiency over the years. Source : Qualcomm, from [1] . . .	2
2.1	Random spatial distribution of interferer nodes.	17
2.2	Clustered PPP. The right image shows the original set of points, and the image on the left shows the clustered points after the transformation.	18
2.3	Annular underlay network. Legend: black dot = interferer nodes, black square = PR, yellow square = PT.	19
3.1	The outage probability vs P_p and P_s , under $\gamma_{Th} = 1$, $\alpha = 2$, $\sigma = 2$, $\sigma_n^2 = 0.001$, $\beta = 0.0001$, $R = 30$, $R_G = 15$, $R_E = 100$	31
3.2	The outage probability vs P_p and P_s , under $\gamma_{Th} = 1$, $\alpha = 2$, $\sigma = 0$, $\sigma_n^2 = 0.001$, $\beta = 0.0001$, $R = 30$, $R_G = 15$, $R_E = 100$	32
3.3	The exact and asymptotic outage probability vs the normalized transmit power P_p , for different values of σ and α under $\sigma_n^2 = 0.001$, $\beta = 0.0001$, $P_s = 30$ dBm, $R = 30$, $R_G = 15$, $R_E = 100$, and $\gamma_{Th} = 1$	33
3.4	The outage probability vs interferer density (β) for different values of σ and α under $P_s = 30$ dBm, $P_p = 70$ dBm, $\sigma_n^2 = 0.001$, $R = 30$, $R_G = 15$, $R_E = 100$, and $\gamma_{Th} = 1$	34
3.5	The outage probability vs interferer density (β) for different values of σ and α under $P_s = 30$ dBm, $P_p R^{-\alpha} = 25$ dBm, $\sigma_n^2 = 0.001$, $R_G = 25$, $R_E = 500$, and $\gamma_{Th} = 1$	35

3.6	The outage probability vs primary transceiver distance (R) for different values of σ and α under $P_s = 30$ dBm, $\gamma_{Th} = 1$, $P_p = 70$ dBm, $R_G = 15$, $R_E = 100$, and $\sigma_n^2 = 0.001$	36
3.7	The CDF of the aggregate interference and the Gamma approximation for different values of β under $P_s = 30$ dBm, $R_G = 15$, $R_E = 100$, $\alpha = 2$, and no shadowing.	37
3.8	The PDF of the Gamma approximated aggregate interference for different values of β under $P_s = 30$ dBm, $R_G = 15$, $R_E = 100$, $\alpha = 2$, and no shadowing.	38
3.9	The PDF of the Gamma approximated aggregate interference for different values of R_G , R_E , and σ under $P_s = 30$ dBm, $\beta = 1 \times 10^{-3}$, and $\alpha = 2$	39
4.1	System model. Legend: Black circle = interferer nodes, black square = PR, $R_2 = 2R$, and $R_M = MR$	42
4.2	Linear interferer network. Legend : black dot = interferer nodes, black square = PR.	48
4.3	Square shaped interferer network. The shaded area contains the interferers. Legend : black square = PR.	50
4.4	System model. Legend: black circle = interferer nodes, black square = PR.	57
4.5	$f_{r_{min}}(x)$ for varying β values when $N \neq 0$	59
4.6	$f_{\frac{r_{min}}{R_G}}(y)$ for varying η values when $N \neq 0$, $\frac{R_E}{R_G} = 4$	60
4.7	System model for a CR setup employing power control. Legend: black circle = nearest interferer node, black square = PR, red square = CR receiver.	62
4.8	The exact and asymptotic outage probability vs the primary system power level P_p , for different values of σ and α under $\beta_l = 0.01$, $R = 20$, and $M = 5$	66

4.9	Comparison of the outage probability vs primary system power level P_p with different values of σ and α , for the multiple-ring model and the annular underlay model under $\beta_l = 0.01$, $R = 20$, and $M = 5$. The values for β , R_G and R_E have been chosen accordingly.	67
4.10	The error percentage of the outage of the multiple-ring model vs the primary system power level P_p , for different values of M and R under $\beta = 0.001$, $\alpha = 2$, and $\sigma = 0$. The value of β_l has been chosen appropriately for each case.	68
4.11	The outage probability vs the primary system power level P_p , under different values of β , for the annular underlay model and the multiple-ring model. $\alpha = 2$, $\sigma = 0$, $R = 5$, and $M = 20$	69
4.12	Outage probability vs P_s for power controlled interferer nodes under $R_{CR} = 0$ and $R_{CR} = 275$ for $\beta = 0.0001$, $\alpha = 2$, $R_E = 200$, $R_G = 25$, $R = 30$, $P_{rec} = -30$ dBm, $\gamma_{Th} = 1$, and $\sigma_n^2 = 0.001$	70
4.13	Outage probability vs P_p for different values of R , with $R_E = 500$, $R_G = 50$, $P_s = 20$ dBm, $\beta = 0.0001$, $\alpha = 2$, $\gamma_{Th} = 1$, and $\sigma_n^2 = 0.001$	71
4.14	Outage probability vs R_G for different values of β , with $R_E = 200$, $R = 40$, $P_p = 50$ dBm, $P_s = 30$ dBm, $\alpha = 2$, $\gamma_{Th} = 1$, and $\sigma_n^2 = 0.0005$	72
4.15	Outage probability vs P_s for different values of β and α , with $R_E = 200$, $R_G = 20$, $R = 10$, $P_p = 60$ dBm, $\gamma_{Th} = 1$, and $\sigma_n^2 = 0.001$	73

Abbreviations

Acronym	Meaning
BPP	Binomial Point Process
CAGR	Cumulative Annual Growth Rate
CCDF	Complementary Cumulative Distribution Function
CDF	Cumulative Distribution Function
CLT	Central Limit Theorem
CR	Cognitive Radio
CVRMSE	Coefficient of Variation of Root Mean Square Error
DSA	Dynamic Spectrum Access
DySPAN	Dynamic Spectrum Access Networks
FSL	Free Space Loss
GPS	Global Positioning System
IEEE	Institute of Electrical and Electronic Engineers
ISI	Inter Symbol Interference
ITU	International Telecommunication Union
MGF	Moment Generating Function
MIMO	Multiple Input Multiple Output
NEM	Normalized Error of the Mean
PDF	Probability Density Function
PDP	Power Delay Profile
PPP	Poisson Point Process
PR	Primary Receiver
PT	Primary Transmitter
QoS	Quality of Service
RMSE	Root Mean Square Error
SINR	Signal to Interference and Noise Ratio
WiMAX	Worldwide interoperability for Microwave Access

List of Symbols & Mathematical Notation

Notation	Definition
$k!$	factorial of k
$\binom{n}{k}$	binomial coefficient, n choose k
$\min(a_1, \dots, a_n)$	minimum of all scalars a_i for relevant i
$O(\cdot)$	the remainder in series
$\Gamma(x, a)$	$\int_a^\infty t^{x-1} e^{-t} dt$
$\Gamma(x)$	$\Gamma(x, 0)$
${}_2\mathcal{F}_1(, ; ;)$	Gauss' Hypergeometric function [2, (eq. 9.10)]
${}_2\mathcal{F}_2(, ; ;)$	generalized Hypergeometric function [2, (eq. 9.14)]
$\mathcal{K}_\nu(\cdot)$	modified Bessel function of the second kind [2, (eq. 8.407)]
$\lfloor x \rfloor$	the largest integer less than x
$E_n(x)$	$\int_1^\infty \frac{e^{-xt}}{t^n} dt$
$f_X(\cdot)$	probability density function (PDF)
$F_X(\cdot)$	cumulative distribution function (CDF)
$M_X(\cdot)$	moment generating function (MGF)
$E_X[\cdot]$	expectation with respect to X

Chapter 1

Introduction

1.1 Wireless Communications

Wireless communications is one of the most revolutionary engineering breakthroughs of all time, and has grown exponentially in terms of technology and users over the past decades. Today, wireless communications has enabled a variety of applications and standards including [3]:

- | | |
|---------------------------------|-----------------------------|
| 1. Mobile telephony | 2. Broadcast technology |
| 3. Wireless Local area networks | 4. Fixed wireless access |
| 5. Cordless telephony | 6. Wireless sensor networks |
| 7. Satellite communications | 8. Radar and navigation |
| 9. Body area networks | 10. Personal area networks |

Cisco states that the global wireless data traffic grew 133% in 2011, and that it was higher than anticipated [4]. Furthermore, the International telecommunication Union (ITU) states that by 2012, the global mobile penetration was at 6 billion, which corresponds to 86% of the world's population [5]. Therefore, the demand for services and bandwidth is extremely high. But, the radio frequency spectrum is a finite resource, and has to be utilized efficiently to allow all these services and technologies to operate.

However, the spectral efficiency gains (data rate that can be sent over a unit

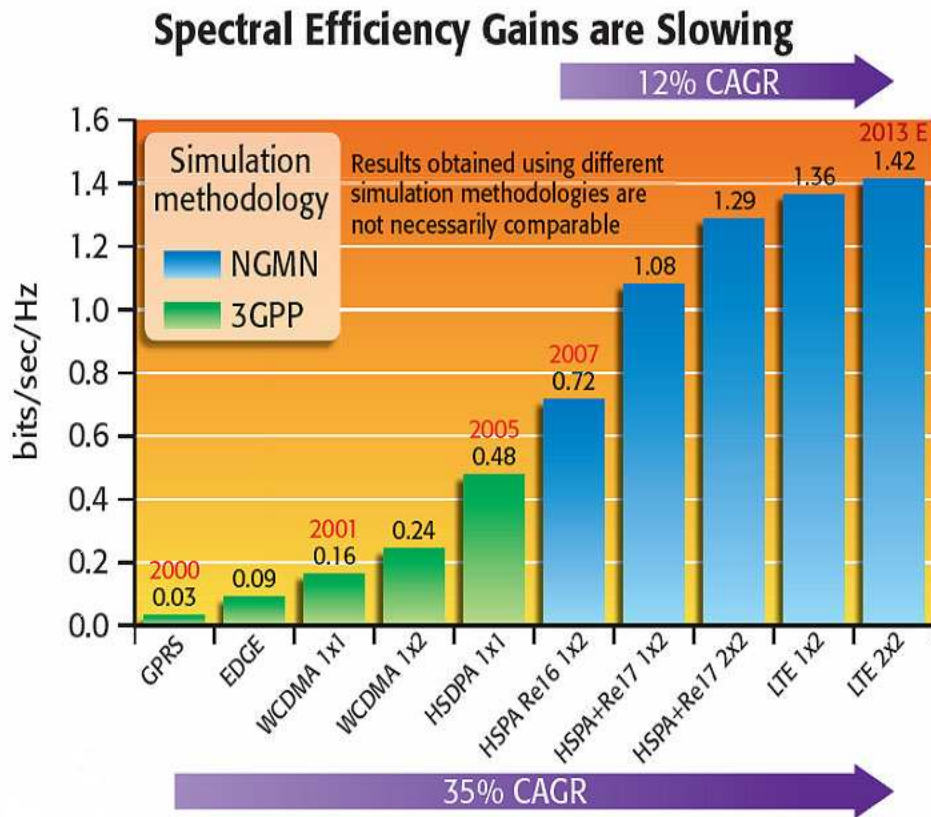


Figure 1.1: Spectral efficiency over the years. Source : Qualcomm, from [1]

bandwidth) are slowing over the years [1]. This slowdown is clearly evident in Fig. (1.1). Due to this, optimizing spectrum usage or developing ways to access pre-allocated spectrum is essential for new technologies.

1.2 Methods to improve spectral efficiency

Several methods to improve spectral efficiency will be discussed next.

1.2.1 Cognitive radio

Many spectrum bands have already been allocated for different services and providers. However, most of pre-allocated frequency spectrum has been found to remain idle for much of the time [6]. This is a significant under utilization of available spec-

trum, and can be mitigated via cognitive radio (CR) [7]. A CR node is a transmitting entity which adapts its system parameters (e.g. frequency, power, multiple access method, modulation) to suit its environment [3]. However, the most well known attribute of CR is the ability to access spectrum pre-allocated to a licensed user. This ability improves spectral efficiency.

In CR terminology, the licensed users are also called primary users. They have reserved the particular frequency block from the governing authorities after paying a fee, and are thus licensed to transmit. The users who opportunistically access primary users' spectrum are termed the secondary users or cognitive radios. While they are permitted to opportunistically access the spectrum, their interference on the primary network should be either eliminated or managed below a prescribed level.

Cognitive radios can be broadly classified based on the access technology into interweave CR networks, spectrum overlay CR networks, and spectrum underlay CR networks [8–12]. However, other literature [10] classify CR networks into just underlay and overlay networks.

- Interweave networks

In interweave CR networks, the secondary users sense the spectrum, and transmit only when primary user transmissions are absent. The spectrum access is thus opportunistic, and requires advanced spectrum sensing schemes in order to begin and end transmissions immediately as necessitated [11]. Instead of spectrum sensing, CR nodes may also use an out-of-band beacon transmission [13] from the primary network to detect the presence or absence of primary transmissions.

- Underlay networks

In spectrum underlay CR networks, the secondary users are allowed to transmit even while primary users are transmitting [8, 10, 11]. To minimize or eliminate interference to the primary network, several schemes have been proposed. The first method is to have a centralized database with dynamic information on the transmitters/receivers of the target frequency in a given area. Therefore, the secondary users can transmit below a certain power level

if they are beyond a given distance. Due to this distance, the secondary user signals attenuate sufficiently so that interference on the primary receiver is negligible. The second method is to use a beacon transmitter from either the primary transmitter or receiver, where the secondary users transmit only when the beacon signal power is less than a certain amount (so that the secondary user is beyond a pre-determined distance). Alternatively, Global Positioning System (GPS) based schemes and spread spectrum schemes have been proposed for underlay networks [8, 10]. Interference generated by underlay networks is the main focus of this thesis.

- **Overlay networks**

Concurrent primary and secondary transmissions are also allowed in overlay CR networks. However, the differing assumption from underlay networks is that the CR nodes have prior information on primary transmissions such as codebook information and channel gains [10, 11]. Moreover, the CR nodes can actively assist the primary transmissions by using a portion of their power to relay primary user messages.

Standards

Since CR is a new technology, no previous standard existed for opportunistic spectrum access. While elements of CR are already included in standards such as IEEE 802.11 (WiFi), IEEE 802.15.4 (Zigbee), and IEEE 802.16 (WiMAX) [14], IEEE 802.22, the Wireless Regional Area Network (WRAN) standard [15] is the first to fully incorporate CR techniques. Furthermore, the IEEE Dynamic spectrum access networks (DySPAN) committee has developed the IEEE P1900.X standards.

IEEE 802.22 has been developed to access white spaces in television frequency bands in order to provide wireless broadband access to rural areas. With this standard, the CR users must be aware about the availability of spectrum at a given instance. The two methods used for spectrum awareness are geo location/database and spectrum sensing [15]. In addition, they should be able to dynamically adapt transmissions to not interfere with licensed TV transmissions [15].

The IEEE P1900.x standards develop better dynamic spectrum access (DSA),

which includes new techniques for managing interference, sensing, network management and coordination of wireless networks [14]. For example, the IEEE P1900.6 standard is regarding spectrum sensing techniques for CR [16]. Furthermore, policies regarding DSA are being developed for current technologies such as 3G/4G, and WiFi [14].

1.2.2 Heterogeneous networks

Heterogeneous networks, another approach to improve spectral efficiency, is a broad concept where different cells co-exist dynamically while using similar frequencies [17]. The cells differ in terms of sizes and power levels drastically. For example, large macro cells (covering a radius of many kilometres) are needed for basic coverage needs and moving subscribers. In contrast, picocells (put in place by the operators to cover a radius of a few hundred metres or less) may be deployed in dense urban areas to increase capacity. Femtocells (which have a small coverage area, and are restricted to a certain building or customer premises) which are even smaller may be used in individual buildings where an extremely high capacity is needed [18]. When services from different cells are available, the user may choose the best cell or use multiple cells to increase their data rate and lower the outage. The performance of heterogeneous networks critically depend on mutual interference levels of the cells.

1.2.3 Small cell networks

The concept of small cells deals with the dense deployment of cells within a given geographical area to increase the capacity, spectral efficiency, and power usage [19]. They are especially useful in urban environments where the demand for wireless data traffic is high. Apart from the obvious spectrum efficiency gains, small cells can potentially provide significant energy savings [19]. However, administration, organization, and maintenance of small cell networks are a challenge. Furthermore,

interference mitigation among different cells and guaranteeing a required Quality of Service (QoS) are demanding [19].

1.3 Problem Statement

While all these techniques improve the overall spectrum efficiency, this thesis will concentrate on underlay CR networks. The advantages of underlay networks are their ability to access the frequency spectrum simultaneously with primary users, and not requiring the secondary users to have a prior knowledge of primary transmissions [11]. Despite these advantages, interference on the primary users due to simultaneous primary and secondary transmissions must be minimized. Therefore, the aggregate interference generated by underlay networks must be characterized for differing operational conditions.

A comprehensive analysis of interference for different channel models, CR node densities, and their spatial distributions is therefore necessary. Furthermore, due to the complexity of existing interference models, simpler, and accurate models are desirable. Therefore, characterizing the aggregate interference and developing approximate models are the main focuses of this thesis.

1.4 Contributions and Outline

The main contributions of the thesis are regarding the analysis, approximation, and modeling of aggregate interference (I). They are broadly listed below:

- Analysis of I for an underlay network consisting of a Poisson process of interfering nodes in a finite annular area around the primary network.
- Development of a Gamma model for I under a composite fading channel via a moment matching method.
- Development of a multiple-ring model for I , and investigation of its accuracy.

- Characterization of the interference caused by the nearest interfering node, and investigation of when the nearest interferer can approximate I .

The outline of the thesis is as follows:

Chapter 2

In Chapter 2, basic background concepts and models for small scale fading, shadowing, path loss, spatial distribution, and others will be presented.

Chapter 3

The first part of Chapter 3 comprises a comprehensive interference analysis for interfering nodes spatially distributed as a Poisson point process in an annular region. The moment generating function (MGF) of the aggregate interference is derived for generic path loss exponent values and shadowing levels. The cumulative distribution function (CDF) of the signal to interference and noise ratio (SINR) is obtained, and an asymptotic analysis is performed. Subsequently, the aggregate interference is modeled by a Gamma distribution using a moment matching method. The accuracy of this approximation is confirmed, and further calculations are facilitated by this simple probability density function (PDF) to represent the aggregate interference.

Chapter 4

Chapter 4 proposes a new model for interference, and also analyzes the effect of the nearest interfering node. In the first part of the chapter, a new system model to approximate the conventional annular underlay model is proposed. The new model, named the multiple-ring model, consists of interferers constrained on multiple rings around the primary receiver (PR) instead of being spread spatially. This model is shown to be accurate, simple, and versatile. It can even be used as a stand-alone system model for other types/shapes of node distributions. In order to evaluate the accuracy, an MGF based performance analysis and an asymptotic analysis is performed for Rayleigh fading, and composite fading and shadowing.

In the second part, the nearest node approximation for the aggregate interference is investigated. The PDF of the distance of the nearest interfering node to the PR, and the MGF of the interference from the nearest node are derived for Rayleigh fading. The nearest node dominates the aggregate interference under certain conditions, which include lower node densities and higher path loss exponent values.

Chapter 2

Background

This chapter provides some brief mathematical background on key concepts used in the thesis. They include wireless channel characterization, spatial distribution models, and interference characterization.

2.1 The wireless channel

Characterizing the wireless channel is extremely important. In this section, channel impairments such as multipath propagation, the Doppler effect, small scale fading, shadowing, and path loss will be discussed briefly.

2.1.1 Multipath fading and the Doppler effect

Due to multiple obstructions and scatterers in the wireless channel, the received signal is the superposition of many signals with different time delays and phases [20]. These multiple copies will cause Inter symbol Interference (ISI), and will severely degrade the performance of the receiver.

The received signal may be represented as [20]

$$r(t) = \mathcal{R} \left\{ \sum_{n=0}^{N(t)} \alpha_n(t) u(t - \tau_n(t)) e^{j(2\pi f_c(t - \tau_n(t)) + \phi_{D_n})} \right\}, \quad (2.1)$$

where $u(t)$ is the complex envelope of the transmitted signal, α_n is the channel gain

for the n -th multipath component, $N(t)$ is the number of resolvable multipath components, $\tau_n(t)$ is the time delay for the n -th component, f_c is the carrier frequency, and ϕ_{D_n} is the Doppler phase shift.

The power delay profile (PDP) represents the average power associated with a given multipath delay (τ) [20]. The average delay and the root mean square (r.m.s.) delay are important statistics of a wireless channel. They are defined as

$$\mu_\tau = \frac{\int_0^\infty \tau P_\tau d\tau}{\int_0^\infty P_\tau d\tau}, \text{ and } \sigma_\tau = \sqrt{\frac{\int_0^\infty (\tau - \mu_\tau)^2 P_\tau d\tau}{\int_0^\infty P_\tau d\tau}}, \quad (2.2)$$

respectively. If the time period of a transmitted signal is defined to be T_s , frequency flat fading occurs if $T_s \gg \sigma_\tau$. Otherwise, the signal would experience frequency selective fading which is not desirable. The term coherence bandwidth is usually defined as

$$B_{coh} \approx \frac{1}{\sigma_\tau}, \quad (2.3)$$

which is roughly the frequency range in which a signal experiences frequency flat fading.

The time variation of the channel is described by the Doppler effect, which is caused by the relative frequency shift between the received signal and the transmitted signal. If the transmitter and receiver are stationary, the Doppler shift is zero. However, when the transmitter and/or receiver move/moves, the maximum Doppler shift is given by

$$f_d = \frac{f_c v}{c}, \quad (2.4)$$

where f_c is the signal frequency, v is the relative velocity between the transceivers, and c is the speed of light. The Doppler spectrum of the channel represents the power associated with a particular Doppler shift (between 0 and f_d). In a similar manner to the PDP, the average and the r.m.s. Doppler spread can be calculated. Furthermore, the coherence time T_{coh} is defined to be approximately $\frac{1}{B_d}$, where B_d is the Doppler spread. If the signal period $T_s \ll T_{coh}$, the signal is said to undergo slow fading. Otherwise, the signal undergoes fast fading.

2.1.2 Small scale fading models

Small scale fading is the random fluctuation of signal amplitude over short distances, and occurs due to the effects of multipath propagation. Small scale fading can be characterized by various mathematical models. The best model for a given channel depends on its characteristics.

Rayleigh fading

Rayleigh fading is the most common model to represent wireless channels including broadcast and mobile systems. Popular due to its mathematical tractability, this model is valid when there is no line-of-sight path between the transmitter and receiver [20]. The probability density function (PDF) of the received signal power under this model is given by

$$f_{\gamma}(x) = \frac{1}{\bar{\gamma}} e^{-\frac{x}{\bar{\gamma}}}, \quad 0 \leq x < \infty, \quad (2.5)$$

where $\bar{\gamma}$ is the average received signal power. It should be noted that while the Rayleigh distribution denotes the envelope amplitude, the power is specified by an exponential distribution.

Rician fading

Rician fading occurs when there is a dominant line-of-sight component. This model is especially useful for channels such as satellite links. The PDF of the received signal is [21]

$$f_{\gamma}(x) = \frac{(K+1)}{\bar{\gamma}} e^{-\left(K + \frac{x(K+1)}{\bar{\gamma}}\right)} I_0 \left(2\sqrt{\frac{xK(K+1)}{\bar{\gamma}}} \right), \quad 0 \leq x < \infty, \quad (2.6)$$

where $\bar{\gamma}$ is the average received signal power, K is the ratio between the line-of-sight component power and the power of the other scatterer components, and $I_0(\cdot)$ is the modified Bessel function of the first kind.

Nakagami- m fading

Nakagami- m fading is a model proposed by [22] which fits the empirical measurements of wireless channels. Its PDF is given by

$$f_{\gamma}(x) = \frac{x^{m-1}}{\Gamma(m)} \left(\frac{m}{\bar{\gamma}}\right)^m e^{-\frac{mx}{\bar{\gamma}}}, \quad 0 \leq x < \infty, m > 0.5, \quad (2.7)$$

where m is a parameter describing the severity of fading. The model is versatile; for example, $m = 1$ yields Rayleigh fading, and $m \rightarrow \infty$ yields the no-fading case.

2.1.3 Shadowing

Shadowing is the random variation of signal amplitude due to blockages from large obstacles such as mountains and buildings in the transmission path. The distances in which shadowing occurs depend on the dimensions of the obstacle causing the shadowing effect [20].

Log-normal shadowing

The most common model for shadowing is the log-normal shadowing model. The PDF of the ratio between transmit to receive power ψ is given by [20]

$$f_{\Psi}(\psi) = \frac{\xi}{\sqrt{2\pi}\sigma_{\psi_{dB}}\psi} e^{-\frac{(10\log_{10}(\psi) - \mu_{\psi_{dB}})^2}{\sigma_{\psi_{dB}}^2}}, \quad 0 \leq \psi < \infty, \quad (2.8)$$

where $\xi = \frac{10}{\ln 10}$, $\mu_{\psi_{dB}}$ is the mean of ψ_{dB} , and $\sigma_{\psi_{dB}}$ is the standard deviation of ψ_{dB} .

Because (2.8) is not mathematically tractable readily, several approximations have been proposed. One such approximation is the Gamma model [23, 24], where the two distributions show a close match except in the lower tail region. Another approximation is the mixture Gamma model developed in [25].

Composite shadowing and fading models

As shadowing and fading occurs simultaneously, it is convenient to have the combined channel effect in a single PDF, rather than work with separate distributions. Thus, several composite models incorporating shadowing and fading have been

proposed [21]. Rayleigh-lognormal, and Nakagami-lognormal models have been proposed [26].

However, the log-normal model (2.8) does not lend itself easily for mathematical analysis. Therefore, by approximating (2.8) by a Gamma model, and incorporating Rayleigh fading, [27] has derived the Generalized- K distribution.

According to this distribution, the composite parameter characterizing Rayleigh fading and shadowing has the form $X = X_s X_f$, where X_s and X_f respectively denote shadowing and Rayleigh fading. X_f is modeled as a unit exponential random variable, and thus the PDF of X can be written as [23]

$$f_{X/X_s}(x) = \frac{1}{X_s} e^{-\frac{x}{X_s}}, \quad 0 \leq x < \infty. \quad (2.9)$$

The shadowing component X_s can be modeled as a Gamma random variable, with the PDF

$$f_{X_s}(y) = \frac{1}{\Gamma(\lambda)} \left(\frac{\lambda}{\Omega_s} \right)^\lambda y^{\lambda-1} e^{-\frac{\lambda}{\Omega_s} y}, \quad 0 \leq y < \infty, \quad (2.10)$$

where $\Gamma(x)$ is the Gamma function. It has been shown in [28] that $\lambda = \frac{1}{e^{\sigma^2} - 1}$ and $\Omega_s = \sqrt{\frac{\lambda+1}{\lambda}}$, where σ^2 is the variance of corresponding log-normal shadowing. When expressed in the decibel scale, $\sigma_{dB} = 8.686 \sigma$.

The composite PDF of Rayleigh fading and Gamma shadowing is obtained by averaging (2.9) over (2.10) as [28]

$$f_X(x) = \frac{2}{\Gamma(\lambda)} \left(\frac{b}{2} \right)^{1+\lambda} x^{\frac{1+\lambda}{2}} \mathcal{K}_{\lambda-1}(b\sqrt{x}), \quad 0 \leq x < \infty, \quad (2.11)$$

which is the Generalized- K distribution, where $b = 2\sqrt{\frac{\lambda}{\Omega_s}}$. This composite model will be subsequently used to characterize channels where both fading and shadowing are present.

Gamma approximation to the Generalized- K distribution

However, because the Generalized- K distribution (2.11) may still be cumbersome for analysis, it has been further approximated by a Gamma PDF [29]. The scale and shape parameters of the Gamma distribution have been chosen by moment matching. Therefore, (2.11) can be approximated as

$$f_X(x) = \frac{1}{\theta^k \Gamma(k)} x^{k-1} e^{-\frac{x}{\theta}}, \quad 0 \leq x < \infty. \quad (2.12)$$

The scale and shape parameters θ and k are $(\frac{2}{\lambda} + 1) \Omega_s$ and $\frac{1}{\frac{2}{\lambda} + 1}$, respectively.

2.1.4 Path loss

Path loss is the reduction in signal amplitude over distance between the transmitter and receiver. Path loss variations only occur over large distances [20].

Free space path loss model

The free space path loss (FSL) model is the most simple path loss model. It can be written as

$$FSL = \left(\frac{4\pi d}{\lambda} \right)^2, \quad (2.13)$$

where d is the distance between the transmitter and receiver, and λ is the wavelength of the transmitted signal.

Empirical path loss models

Because free space conditions do not hold for the wireless environment which encompasses many variable factors such as buildings, trees, hills, and houses, the path loss modeling is difficult. Thus, several empirical models have been developed using real world experimental data. These include the Okumura model, Hata model, COST 231 Hata model, and COST 231 Wolfisch-Ikegami model [20].

The COST 231 Hata model for path loss (PL) can be written as [20]

$$\begin{aligned} PL_{dB}(d) = & 46.3 + 33.9\log_{10}(f_c) - 13.82\log_{10}(h_t) - a(h_r) \\ & + (44.9 - 6.55\log_{10}(h_t))\log_{10}(d) + C_M, \end{aligned} \quad (2.14)$$

where h_t is the transmit antenna height, h_r is the receiver antenna height, f_c is the transmit signal frequency, and d is the distance between the transmitter and receiver. For suburbs and small cities, $a(h_r)$ is defined as

$$a(h_r) = (1.1\log_{10}(f_c) - 0.7)h_r - (1.56\log_{10}(f_c) - 0.8). \quad (2.15)$$

C_M is 0 for small cities and suburbs, while it is 3 for large cities.

Simplified path loss model

The most common path loss model used in analysis is the simplified path loss model, and will be used in the subsequent chapters. According to this model, the power at a certain distance r from the transmitter is given by

$$P(r) = P_0 \left(\frac{r_0}{r} \right)^\alpha, \quad (2.16)$$

where P_0 is the observed power at a distance r_0 from the transmitter, and α is the path loss exponent. This model includes the free space path loss model (2.13) as a special case when $\alpha = 2$.

2.1.5 Power control

Power control is the variation of transmit power according to the situation such as distance from the receiver, other users' activities, and channel conditions. Power controlling schemes have a dual benefit of saving transmitter power as well as reducing unwanted interference. They can be based on numerous factors such as QoS feedback from the receiver, distance to the receiver, and locations of other co-channel nodes. Several schemes have been proposed for CR networks [30, 31]. However, this thesis mostly ignores power control schemes, except when a simple power control scheme based on distance to the receiver is considered in Chapter 4.

2.2 Spatial distribution models

Spatial distribution refers to the random locations of interferer nodes in a given area. For interference analysis, modeling the spatial distribution of the interfering nodes (Fig. 2.1) is essential. Several spatial distributions have been used in literature to model the random locations of nodes. The two most popular ones are the Poisson point process [32], and the binomial point process [33]. A point process is a random pattern of points in d -dimensional space (where usually $d = 2$ or $d = 3$

in applications) [34]. For modeling the distribution of interferers, a 2 dimensional space is commonly used.

2.2.1 Poisson point process

The Poisson point process (PPP) is the most common spatial distribution used to model the distribution of interfering nodes in a given area [35–40]. The average number of spatial points in a given area is the intensity. A PPP is termed homogeneous if the intensity parameter is constant. For non-homogeneous PPPs, the intensity parameter is a function of the location. For a 2-dimensional homogeneous spatial PPP, the probability of having n nodes in a region B is given by [33]

$$P(N(B) = n) = \frac{(\lambda v(B))^n}{n!} e^{-\lambda v(B)}, \quad n = 0, 1, 2, \dots \quad (2.17)$$

where λ is the intensity parameter, and $v(B)$ is the area of B . The PPP model used in the thesis will be explained in detail within the following section.

Thinning

Thinning refers to the process of removing certain points from the total set of points [34]. Thinning comes in extremely useful while modeling interference where the whole set of nodes may not be active (not transmitting). In such a scenario, the thinned set of points will model the active nodes. The thinning process occurs by marking the set of points by an indicator random variable I_X (which can take the values 0 or 1), and deleting the points marked with 0. Thinning has two forms: dependent thinning and independent thinning [34]. When I_X are independent random variables, it is independent thinning. In dependent thinning, any point in the PPP which has a neighboring node closer than a certain distance will be deleted.

Clustering

Clustering is the process of taking a set of spatial points \mathcal{A} , and replacing the point A by a random set of points Z_A for each point $A \in \mathcal{A}$ [34]. Fig. 2.2 shows an example for the clustered PPP. Clustering is important when modeling the interfering

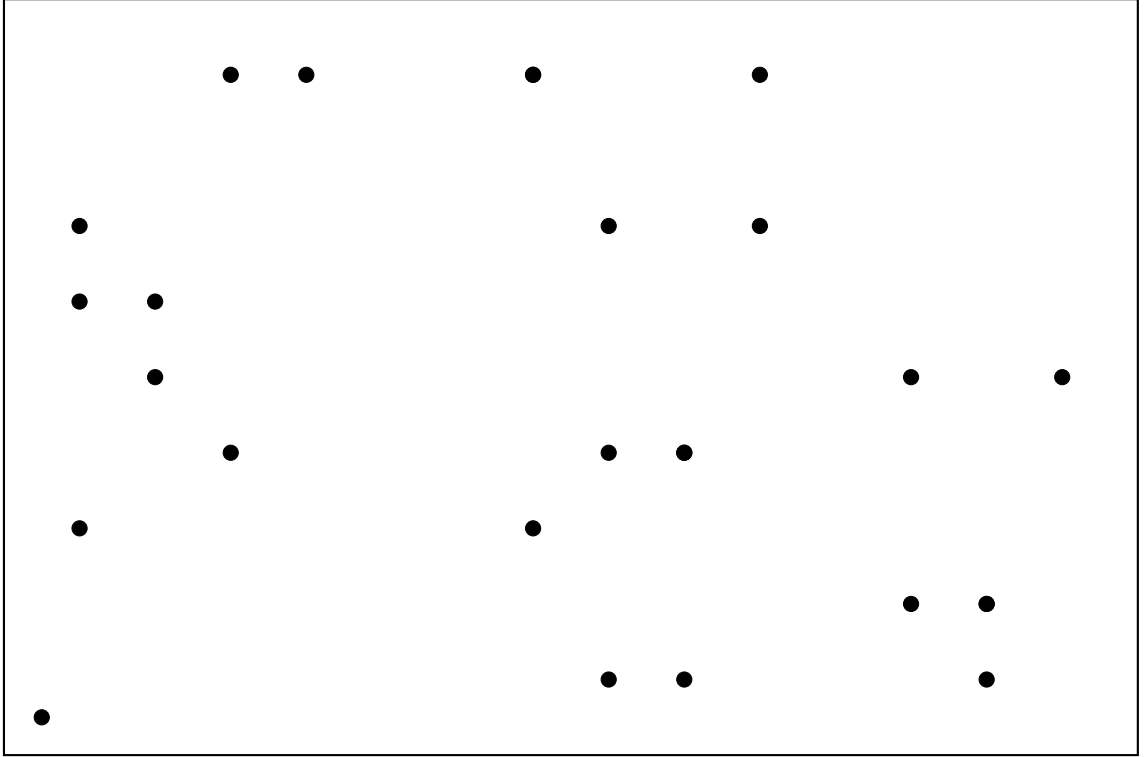


Figure 2.1: Random spatial distribution of interferer nodes.

nodes distributed around secondary base stations. In such a scenario, the secondary base stations will be the original set of points, and the nodes will be the clustered points after the transformation. References [35, 41–43] consider clustering in their analysis.

2.2.2 Binomial point process

The Binomial point process (BPP) is useful to model interferers when the total number of nodes is fixed. Reference [44] argues that the BPP is a better model to represent the spatial distribution of nodes because the total number of nodes is often fixed. For a given area of Z , the total number of nodes in B ($B \in Z$) is given by [45],

$$P(N(B) = n) = \binom{N}{n} p^n (1-p)^{N-n}, \quad n = 0, \dots, N \quad (2.18)$$

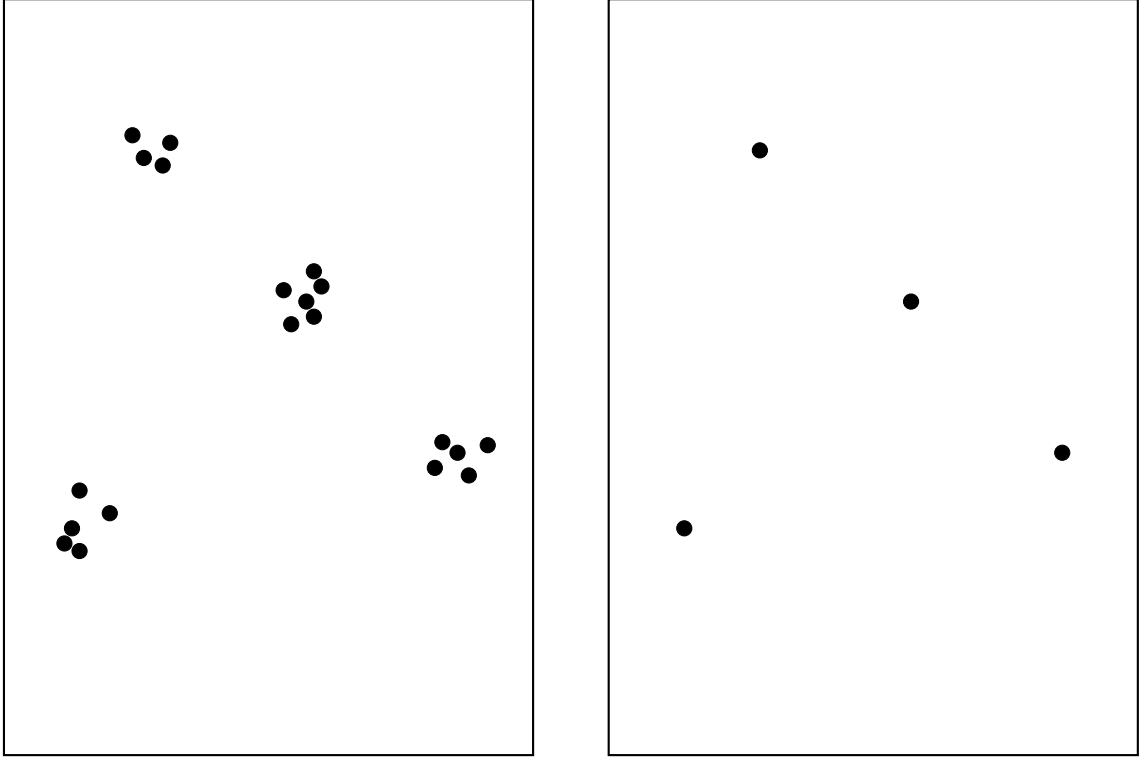


Figure 2.2: Clustered PPP. The right image shows the original set of points, and the image on the left shows the clustered points after the transformation.

where N is the total number of nodes in Z , and $p = \frac{v(B)}{v(G)}$.

2.3 Annular underlay networks

The importance of CR networks in improving spectral efficiency was discussed in Chapter 1. However, although underlay CR nodes are intelligent, residual interference to the primary system is unavoidable. A comprehensive understanding of the aggregate interference is critical when designing interference management schemes. Interference analysis in cognitive radio networks has thus been a hot research topic in recent times [30,46–53]. One method which has been used to reduce the interference in an underlay network is the use of an exclusion region (contention control) [30, 54, 55] . In such a setup, nodes in an exclusion zone around the primary transmitter or receiver are not permitted to transmit, and nodes outside this

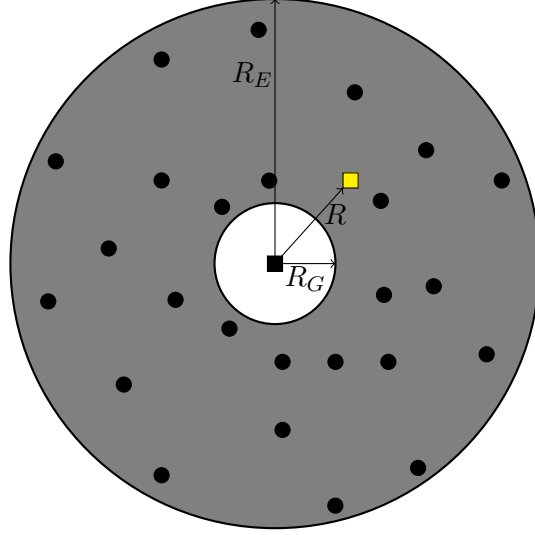


Figure 2.3: Annular underlay network. Legend: black dot = interferer nodes, black square = PR, yellow square = PT.

zone are permitted to transmit below a certain power level. As discussed in Chapter 1, this process may be enabled by a beacon signal from the primary transmitter or receiver, prior location knowledge, or Global Positioning Systems. In a beacon setup, if the beacon is from the primary transmitter or from the primary receiver, the exclusion region would be around the transmitter or receiver respectively. We will be considering an exclusion region around the PR.

Although interferers can be distributed over arbitrary shaped regions, analysis of such may be intractable. Furthermore, the interferers may be located in a polygon shaped area (e.g. square or hexagonal). An annular region (Fig. 2.3) [49, 50, 56, 57] is a good approximation for arbitrary and polygon shaped distributions, and is mathematically conducive for further analysis.

The interferer nodes form an underlay CR network which is intelligent enough to adhere to the exclusion region around the PR. This region has an inner radius (guard distance) of R_G and an outer radius of R_E . The guard distance ensures a minimum performance on the PR. The interference from the nodes beyond R_E is assumed to be negligible due to path loss. An infinite region ($R_E \rightarrow \infty$) is a special case of the model.

The primary transmitter (PT) to PR distance is denoted as R , and it doesn't

depend on the guard distance. The number of interferer nodes N is random. The nodes are distributed according to a homogeneous Poisson point process which has the distribution of (2.17), where β is the interferer density, and $A_I = \pi(R_E^2 - R_G^2)$ is the total area encompassing the interferer nodes ($v(B)$). Non-homogeneous situations will be application or geography specific, and thus not very useful for a general analysis.

Not all interferer nodes may be active at a given time, and some may be inhibited from transmitting due to interference between the CR nodes themselves. However, an ad-hoc network of interferer nodes where all the nodes concurrently engage in transmission is assumed. Our results thus give a worst-case upper bound for the aggregate interference and outage when interferer nodes use a medium access control protocol. Such cases however can be handled by introducing an activity factor. Conversely, without the loss of generality, we can consider β as the density of all the active nodes.

For the purposes of this thesis, we will only consider one PR, and that other PRs are located a sufficient distance away. If the next closest PR is less than $2R_G$ away from the PR under consideration, the exclusion region will be of a complex shape. Furthermore, if it is less than a distance of $2R_E$ away, the interferer area will not be annular. However, these considerations are out of the scope for this thesis.

2.3.1 Aggregate interference

The aggregate interference experienced at the primary receiver is the sum of interference from all the active interferer nodes transmitting in the same frequency spectrum block. Therefore, the aggregate interference I can be written as

$$I = \sum_{i=1}^N I_i, \quad (2.19)$$

where I_i is the interference caused by the i -th interferer, and N is the number of interferers.

As the PDF of the aggregate interference is intractable, this thesis develops an MGF based approach. The MGF can be obtained relatively easily because, for a

sum of independent interferers, the total MGF would be the multiplication of each interferer's individual MGF. The MGF $M_I^i(s)$ of the interference from a single node can be written as

$$M_I^i(s) = E[e^{-sI_i}], \quad (2.20)$$

where $E[\cdot]$ denotes the expectation, and s is the Laplace variable. The aggregate interference is dependent upon various factors. They include the channel parameters such as path loss, shadowing, and small scale fading. Furthermore, power controlling schemes and transmit powers of the nodes, the spatial distribution of nodes, and the design of exclusion regions also play a vital role. The sensing procedures of the beacon transmission/ frequency spectrum and missed detection of these by the nodes also need to be considered.

Modeling of aggregate interference to fit well known distributions has been extremely popular due to the intractability of exact analysis. These include approximation by Gaussian distributions, log-normal distributions, tailed α -stable distributions, and as a sum of normal and log-normal distributions [58–61].

In the following chapters, several different models for the aggregate interference will be developed.

2.4 Conclusion

This section provided background material for the thesis. Fading and shadowing models, spatial distributions, and the annular underlay network model were described.

Chapter 3

Aggregate Interference Analysis

Chapter 2 provided introductions and justifications to the system model, and explained the need to characterize aggregate interference. This chapter develops an exact analysis and a Gamma approximation of the aggregate interference for the annular underlay network model introduced in Section 2.3.

3.1 Introduction

In Chapter 2, the annular underlay model for investigating the aggregate interference was presented. The random aggregate interference depends on several factors such as channel parameters, spatial distribution of the interferer nodes, activity factors, and power control. These parameters were briefly described in Chapter 2.

As the modeling of aggregate interference at the primary receiver (PR) is critical to characterize performance degradation, it has received much attention recently. Reference [56] analyzes the average aggregate interference when transmission constraints among CR nodes are considered, while [57] analyzes the capacity-outage of a CR network due to aggregate interference. Reference [58] shows that under certain conditions, the aggregate interference is not lognormal. In reference [59], the authors suggest that the aggregate interference can be modeled as the sum of a normal random variable and a lognormal random variable. Reference [52] considers different activity models for the CR nodes and obtains cumulants of the aggregate interference by using Campbell's theorem. Reference [49] derives the moment

generating function (MGF) of the combined interference without shadowing for a number of different path loss exponent values.

The aggregate interference will be investigated further in the subsequent sections. First, the moment generating function of the aggregate interference will be derived for the annular underlay model (Fig. 2.3). The exact and asymptotic outage performance will be analyzed. Second, the aggregate interference will be modeled with a Gamma model.

3.2 Aggregate interference of annular underlay networks

3.2.1 Introduction

This section provides a comprehensive analysis of the aggregate interference for the annular underlay model (Fig. 2.3). The analysis considers all relevant channel impairments. The interfering signals are assumed to undergo composite fading and shadowing, and path loss (arbitrary exponents). The exact closed-form MGFs of the aggregate interference for both the generalized- K distribution, and the Gamma approximation to it are derived. Closed-form expressions for the outage and an asymptotic performance analysis are provided.

3.2.2 System model

The system model of Fig. (2.3) is used for the analysis, with the same parameters.

From the simplified path loss model, the received power at distance r from the transmitter is given by (2.16). For brevity, we define the quantity $P_0 r_0^\alpha$ to be the power level of the transmitter (which depends on the transmit power, gains, and frequency). The total interference power received at the PR is given by (2.19). The

interference power I_i is given by

$$I_i = P_s r_i^{-\alpha} X_i, \quad (3.1)$$

where P_s is the power level of an interferer, and r_i is the distance between the i -th interferer and PR. P_s is a constant, and no power control occurs. X_i characterizes the combined effects of small-scale fading and shadowing. The PDF of X_i follows the Generalized- K distribution of (2.11).

3.2.3 Interference Statistics

In this subsection, the exact MGF of the aggregate interference and an approximate MGF to the aggregate interference are derived.

MGF of the aggregate interference

Because r_i and X_i are independent, the MGF $M_I^i(s)$ of the i -th interferer ($i = 1 \dots N$) is given by (2.20),

$$M_I^i(s) = E_{X_i, r_i}[e^{-sI_i}] = E_{X_i}[E[e^{-sI_i}]]. \quad (3.2)$$

For the homogeneous PPP considered, the CDF of r_i when $R_G < r_i < R_E$ can be written as

$$\begin{aligned} F_{R_i}(r_i) &= P(R_i < r_i) \\ &= \frac{r_i^2 - R_G^2}{R_E^2 - R_G^2}. \end{aligned} \quad (3.3)$$

Therefore, the PDF of r_i can be obtained by differentiating the CDF as

$$f_R(r_i) = \begin{cases} \frac{2\pi r_i}{A_I} & , R_G < r_i < R_E \\ 0 & , \text{otherwise} \end{cases}. \quad (3.4)$$

By averaging e^{-sI_i} using the the PDF of interferer distance (3.4), we get

$$\begin{aligned} M_{I/X_i}^i(s) &= \int_{R_G}^{R_E} e^{-sP_s r^{-\alpha} X_i} \left(\frac{2\pi r}{A_I} \right) dr \\ &= \frac{2\pi}{A_I} \int_{R_G}^{R_E} e^{-(sP_s X_i) r^{-\alpha}} r dr \\ &= \frac{2\pi}{\alpha A_I} \left(R_E^2 E_{\frac{2+\alpha}{\alpha}} \left(\frac{P_s s X_i}{R_E^\alpha} \right) - R_G^2 E_{\frac{2+\alpha}{\alpha}} \left(\frac{P_s s X_i}{R_G^\alpha} \right) \right), \end{aligned} \quad (3.5)$$

where $E_n(x)$ is the generalized exponential integral. Averaging further respect to the composite fading model (2.11), the MGF of the interference from the i -th interferer is derived as

$$M_I^i(s) = \frac{\pi (P_s s)^{\frac{2}{\alpha}-2} b^{-\frac{4}{\alpha}-2}}{(-1)^{\lambda+\frac{2}{\alpha}} 4\alpha^2 (1+\alpha) \Gamma(\lambda) A_I} (\mathcal{Q}(R_E) - \mathcal{Q}(R_G)), \quad (3.6)$$

where $\mathcal{Q}(R)$ is defined as

$$\begin{aligned} \mathcal{Q}(R) &= \frac{b^{4+\frac{4}{\alpha}} (-1)^{\frac{2}{\alpha}+\lambda} \alpha^2 \Gamma(\lambda-1) R^{2\alpha+2}}{(P_s s)^{\frac{2}{\alpha}}} {}_2\mathcal{F}_2\left(2, 2 + \frac{2}{\alpha}; 3 + \frac{2}{\alpha}, 2 - \lambda; \frac{R^\alpha b^2}{4P_s s}\right) \\ &+ \frac{2^{5+\frac{4}{\alpha}} (P_s s)^2 (1+\alpha) \pi}{\sin(\pi\lambda)} \\ &\times \left((2+\alpha) \Gamma\left(1 + \lambda + \frac{2}{\alpha}\right) \right. \\ &\left. + \alpha \left(\lambda \Gamma\left(1 + \lambda + \frac{2}{\alpha}, -\frac{R^\alpha b^2}{4P_s s}\right) - \Gamma\left(2 + \lambda + \frac{2}{\alpha}, -\frac{R^\alpha b^2}{4P_s s}\right) \right) \right). \quad (3.7) \end{aligned}$$

The special functions ${}_2\mathcal{F}_2(, ; ;)$ and $\Gamma(x, a)$ are the generalized Hypergeometric function and the upper incomplete Gamma function respectively [2]. Due to the complexity of (3.6), an accurate approximation is desirable. To this end, the Gamma approximation to the generalized- K distribution (2.12) can be used.

Using this approximation, we get $M_{I,approx}^i(s)$ as

$$M_{I,approx}^i(s) = \frac{1}{2+k\alpha} \left(\frac{2\pi}{A_I \theta^k} \right) \left(\frac{R_E^{\alpha k+2}}{(P_s s)^k} \mathbb{I}\left(\frac{R_E^\alpha}{P_s s \theta}\right) - \frac{R_G^{\alpha k+2}}{(P_s s)^k} \mathbb{I}\left(\frac{R_G^\alpha}{P_s s \theta}\right) \right). \quad (3.8)$$

where $\mathbb{I}(x)$ is given by

$$\mathbb{I}(x) = {}_2\mathcal{F}_1(k, k+2/\alpha; 1+k+2/\alpha; -x), \quad (3.9)$$

and ${}_2\mathcal{F}_1(, ; ;)$ is the Gauss' Hypergeometric function [2].

Because each interferer is assumed to be independent, the MGF of I given N can be written as

$$M_{I/N}(s) = \prod_{i=1}^n M_I^i(s) = (M_I^i(s))^n. \quad (3.10)$$

By averaging $M_{I/N}(s)$ over the probability distribution (2.17), we find

$$M_I(s) = \sum_{n=0}^{\infty} M_{I/N}(s) \frac{(\beta A_I)^n}{n!} e^{-\beta A_I}. \quad (3.11)$$

Substituting (3.10) into (3.11), we get

$$M_I(s) = e^{\beta A_I (M_I^i(s)-1)}. \quad (3.12)$$

3.2.4 Performance Analysis

This section derives the outage probability, the asymptotic outage and the diversity/coding gains.

Receiver SINR characteristics

Here, we derive the CDF and the PDF . The SINR γ at the PR can be written as

$$\gamma = \frac{P_p R^{-\alpha} Y}{I + \sigma_n^2}, \quad (3.13)$$

where P_p is the power level of the PT, σ_n^2 is the noise variance, and Y is the channel gain between the primary transmitter and receiver. We only consider the case where the primary signals undergo path loss and Rayleigh fading due to the mathematical complexity of analyzing for other cases. Then, Y is a unit exponential PDF with the distribution of (2.5). The variables Y and I are independent, and the CDF of γ is

$$\begin{aligned} F_{\gamma/I}(x) &= P\left(\frac{P_p R^{-\alpha} Y}{I + \sigma_n^2} \leq x\right) \\ &= P\left(Y \leq \frac{x(I + \sigma_n^2)}{P_p R^{-\alpha}}\right) \\ &= 1 - e\left(-\frac{x(I + \sigma_n^2)}{P_p R^{-\alpha}}\right). \end{aligned} \quad (3.14)$$

Averaging with respect to I , we get

$$\begin{aligned} F_\gamma(x) &= 1 - e\left(-\frac{x\sigma_n^2}{P_p R^{-\alpha}}\right) E_I \left[e^{-I\left(\frac{x}{P_p R^{-\alpha}}\right)} \right] \\ &= 1 - e\left(-\frac{x\sigma_n^2}{P_p R^{-\alpha}}\right) M_I \left(\frac{x}{P_p R^{-\alpha}} \right). \end{aligned} \quad (3.15)$$

Substituting γ_{Th} instead of x gives the outage equation, where γ_{Th} is the threshold SINR level for the PR.

The PDF $f_\gamma(x)$ can be obtained by differentiation of (3.15) as

$$f_\gamma(x) = \left(A - \frac{BV}{x} \left(\frac{H(k + \frac{2}{\alpha})}{(Ux + J)^k} - \mathbb{I}\left(\frac{J}{Ux}\right) + \frac{Hk}{(Ux)^k} \mathbb{I}\left(\frac{J}{Ux}\right) - \frac{F(k + \frac{2}{\alpha})}{(Ux + G)^k} + \mathbb{I}\left(\frac{G}{Ux}\right) - \frac{Gk}{(Ux)^k} \mathbb{I}\left(\frac{G}{Ux}\right) \right) \right) \times e^{\left(-B - Ax + BV \left(\frac{F}{(Ux)^k} \mathbb{I}\left(\frac{G}{Ux}\right) - \frac{H}{(Ux)^k} \mathbb{I}\left(\frac{J}{Ux}\right) \right)\right)}, \quad (3.16)$$

where $A = \frac{\sigma_n^2}{P_p R^{-\alpha}}$, $B = \beta A_I$, $U = \frac{1}{P_p R^{-\alpha}}$, $V = \frac{1}{2+k\alpha} \left(\frac{2}{A_I \theta^k} \right)$, $F = \frac{R_E^{\alpha k+2}}{P_s^k}$, $G = \frac{-R_E^\alpha}{P_s \theta}$, $H = \frac{R_G^{\alpha k+2}}{P_s^k}$ and $J = \frac{-R_G^\alpha}{P_s \theta}$.

Asymptotic Outage

Since the outage probability (3.15) is complicated, a mathematically tractable asymptotic expression is useful. An asymptotic outage probability expression is derived for, when $\frac{P_p}{T}$ is significantly larger than P_s and σ_n^2 . By expanding $\mathbb{I}(\mathcal{C}x)$, we can obtain

$$\mathbb{I}(\mathcal{C}x) = \frac{2 + \alpha k}{2x^k \mathcal{C}^k} + \frac{k(2 + \alpha k)}{x^{k+1} \mathcal{C}^{k+1} (\alpha - 2)} + O\left(\frac{1}{x^{k+2}}\right), \quad (3.17)$$

where \mathcal{C} is a constant. Thus, by using (3.17), for the expression of the MGF (3.8) in (3.15), and with some algebraic manipulations, the CDF for high $\frac{P_p}{\gamma T h}$ with respect to the noise and interference can be obtained as

$$F_{\gamma_{Asy}}(x) = 1 - e^{\left(-\frac{x\sigma_n^2}{P_p R^{-\alpha}}\right)} e^{\frac{2\beta\pi\theta k R^\alpha P_s}{\alpha-2} \frac{P_s}{P_p} (R_E^{2-\alpha} - R_G^{2-\alpha}) x}. \quad (3.18)$$

For small x , e^x can be written as $1 + x$. Therefore, (3.18) can be approximated by

$$F_{\gamma_{Asy}}(x) = 1 - \left(1 - \frac{x\sigma_n^2}{P_p R^{-\alpha}}\right) \times \left(1 + \frac{2\beta\pi\theta k R^\alpha P_s}{\alpha-2} \frac{P_s}{P_p} (R_E^{2-\alpha} - R_G^{2-\alpha}) x\right). \quad (3.19)$$

Defining $\mathcal{A} = \frac{\sigma_n^2}{R^{-\alpha}}$ and $\mathcal{B} = \frac{2\beta\pi\theta k R^\alpha}{\alpha-2} P_s (R_E^{2-\alpha} - R_G^{2-\alpha})$, we get

$$F_{\gamma_{Asy}}(x) = 1 - \left(1 - \mathcal{A} \frac{x}{P_p}\right) \left(1 + \mathcal{B} \frac{x}{P_p}\right) \approx (\mathcal{A} - \mathcal{B}) \frac{x}{P_p}, \quad (3.20)$$

which is the asymptotic CDF.

Diversity Gain and Coding Gain

The diversity gain and coding gain fully characterize the asymptotic performance of a system. The outage probability at high SINR can be written as

$$P_{out}(\gamma) \approx (G_c \gamma)^{-G_d}, \quad (3.21)$$

where G_c is the coding gain and G_d is the diversity gain. Increasing the SINR is analogous to increasing P_p while having a constant σ and P_s . Therefore, P_{out} becomes

$$P_{out} \approx \left(\frac{1}{(\mathcal{A} - \mathcal{B})} \frac{P_p}{x} \right)^{-1}. \quad (3.22)$$

From (3.22), we observe that $G_d = 1$ and $G_c = \frac{1}{(\mathcal{A} - \mathcal{B})T}$.

3.3 Gamma model approximation

3.3.1 Introduction

In the previous section, the exact and approximate MGFs were obtained for the annular underlay model. However, the complexity of these results is high, and even the approximate MGF (3.8) is complicated. Although the CDF (3.15) and PDF (4.6) of the SINR when the primary signals undergo Rayleigh fading were derived, obtaining the CDF and PDF of the aggregate interference (I) itself is extremely difficult. A simple approximation to the aggregate interference PDF will help in the analysis of systems such as multiple antenna (MIMO) systems and relay networks. Therefore, an accurate but simple approximation for the aggregate interference is useful. A proper approximation should be valid under varying inner and outer radii, path loss exponent values, shadowing variances, and node densities. In the rest of this section, the Gamma approximation for I will be derived. The accuracy of the approximation will be described later in the numerical results section.

3.3.2 The Gamma Approximation

The Gamma approximation would use the approximate MGF (3.8) for analytical purposes. Due to the use of Gamma shadowing, the aggregate interference may also follow a Gamma model, rather than a Gaussian model which can be obtained via the use of the Central Limit Theorem. The aggregate interference (2.19) is thus assumed to be modeled by a Gamma random variable. Therefore, the PDF of the aggregate interference I , is given by

$$f_I(x) = \frac{1}{\theta_a^{k_a} \Gamma(k_a)} x^{k_a-1} e^{-\frac{x}{\theta_a}}, \quad (3.23)$$

where k_a is the shape parameter and θ_a is the scale parameter. Suitable values of k_a and θ_a to approximate the distribution of I are needed.

These parameters can be obtained by employing a moment matching method [29]. For the Gamma approximation, the first and second order matching of moments are sufficient to find the shape and scale parameters. Higher order moment matching is not needed.

The first- and second-order statistics of the aggregate interference are important performance means by themselves. $E[I]$, the expected value of the interference is $\beta A_I E[I_i]$, where the interference from a single interferer, I_i is given by

$$I_i = P_s r_i^{-\alpha} X_i. \quad (3.24)$$

Because r_i and X_i are independent, $E[I_i]$ can be written as

$$E[I_i] = P_s E[r_i] E[X_i]. \quad (3.25)$$

After performing the expectations, it can be shown that

$$E[I] = 2\pi P_s \beta \sqrt{e^{\sigma^2}} \left(\frac{R_E^{2-\alpha} - R_G^{2-\alpha}}{2 - \alpha} \right). \quad (3.26)$$

But, there will be a singularity under $\alpha = 2$. Therefore, by applying the L'Hospital's rule, we can obtain $E[I]$ when $\alpha = 2$ as follows;

$$\begin{aligned} E[I]_{\alpha=2} &= 2\pi P_s \beta \sqrt{e^{\sigma^2}} \left[\frac{\frac{d}{d\alpha}(R_E^{2-\alpha} - R_G^{2-\alpha})}{\frac{d}{d\alpha}(2 - \alpha)} \right]_{\alpha=2} \\ &= 2\pi P_s \beta \sqrt{e^{\sigma^2}} (\log(R_E) - \log(R_G)). \end{aligned} \quad (3.27)$$

The variance is defined as,

$$Var[I] = E[I^2] - E[I]^2. \quad (3.28)$$

After obtaining an expression for $E[I^2]$, $Var[I]$ is found out to be

$$Var[I] = \pi\beta P_s^2 k \theta^2 (1+k) \left(\frac{R_E^{2-2\alpha} - R_G^{2-2\alpha}}{1-\alpha} \right). \quad (3.29)$$

The expected value and variance can be matched with those of a Gamma distribution. The expected value and variance of the Gamma distribution are $k_a\theta_a$ and $k_a\theta_a^2$ respectively. Therefore, by matching these moments, the shape parameter and the scale parameter of the Gamma approximation can be found out to be $\frac{(E[I])^2}{Var[I]}$, and $\frac{Var[I]}{E[I]}$ respectively. By substituting $E[I]$ and $Var[I]$, we can find that

$$k_a = \frac{2\pi\beta (1-\alpha) (R_E^{2-\alpha} - R_G^{2-\alpha})^2}{e^{\sigma^2} (2-\alpha)^2 (R_E^{2-2\alpha} - R_G^{2-2\alpha})}, \quad (3.30)$$

and

$$\theta_a = P_s \left(e^{\sigma^2} \right)^{\frac{3}{2}} \frac{(2-\alpha) (R_E^{2-2\alpha} - R_G^{2-2\alpha})}{(1-\alpha) (R_E^{2-\alpha} - R_G^{2-\alpha})}, \quad (3.31)$$

respectively. The accuracy of the approximation, and distribution will be discussed in detail in the numerical results section.

3.4 Numerical Results

This section provides the numerical results, simulations and comparisons of the aggregate interference for the annular underlay model, and the Gamma model of the aggregate interference.

3.4.1 Numerical results of Aggregate interference for annular underlay networks

Here, we show the exact and asymptotic characteristics of the outage probability with the variation of the primary power level, interfering CR power level, and node

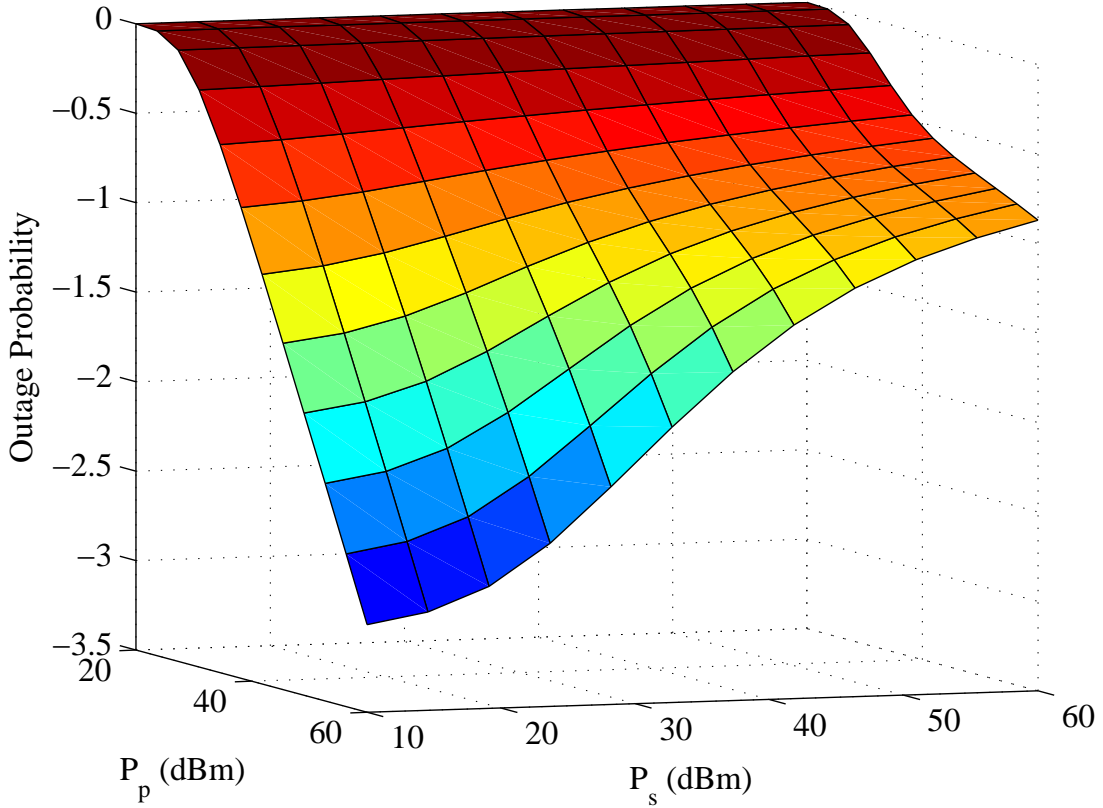


Figure 3.1: The outage probability vs P_p and P_s , under $\gamma_{Th} = 1$, $\alpha = 2$, $\sigma = 2$, $\sigma_n^2 = 0.001$, $\beta = 0.0001$, $R = 30$, $R_G = 15$, $R_E = 100$.

density under differing conditions. A Gamma shadowing environment has been considered for the simulation, and $M_{I,approx}^i$ has been used for our theoretical calculations. When $\sigma \rightarrow 0$, we have the situation where shadowing is negligible.

In Fig. 3.1, the outage probability is plotted with respect to both the primary power level P_p and interferer power level P_s for fixed values of R , R_G , R_E and a noise variance $\sigma_n^2 = 0.001$. It uses free space propagation ($\alpha = 2$), shadowing index $\sigma = 2$, and the interferer density $\beta = 0.0001$. The outage probability decreases slowly at high P_s and, approaches the noise limited scenario for low P_s values. Even if P_p is increased, if P_s increases correspondingly, the outage probability remains unchanged.

Fig. 3.2 depicts the same scenario of Fig. 3.1 except for the fact that in this case, the shadowing variance $\sigma = 0$. It is interesting to observe that at higher P_s ,

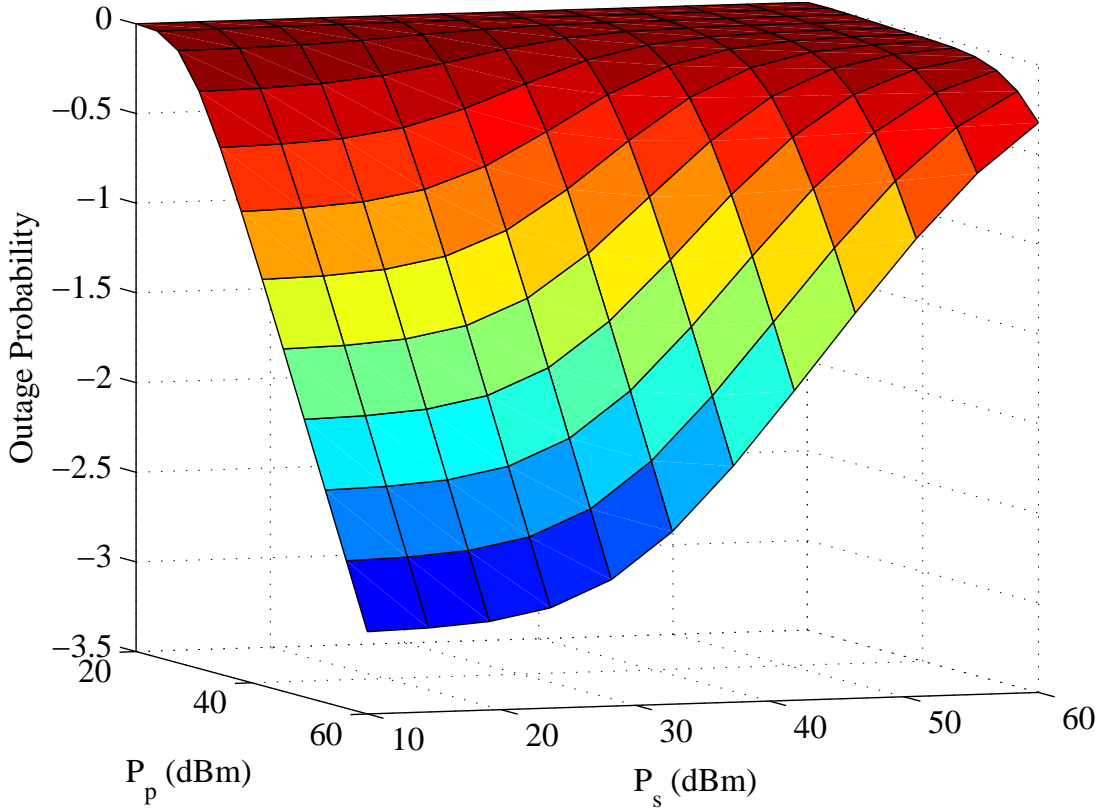


Figure 3.2: The outage probability vs P_p and P_s , under $\gamma_{Th} = 1$, $\alpha = 2$, $\sigma = 0$, $\sigma_n^2 = 0.001$, $\beta = 0.0001$, $R = 30$, $R_G = 15$, $R_E = 100$.

the $\sigma = 0$ plot has worse performance and vice versa at lower P_s .

Fig. 3.3 shows the exact and the asymptotic outage probability with respect to P_p for differing levels of shadowing and path loss exponents. At high P_p , the asymptotic curves are a perfect match to the exact outage plots. An important observation is that at this interferer node density, when the path loss exponent increases, shadowing has little effect on the outage. When the path loss exponent is 4, the plots for both shadowing index values show little difference; however, under free space propagation, the plots vary significantly for the two different σ values. This result is consistent with the derivation obtained earlier in (3.22). For the values for R_G , R_E and R that we selected, the outage probability increases with α . If $R \ll R_G$, a higher α will ensure a lower outage probability.

Fig. 3.4 compares the outage probability when the interferer density β varies,

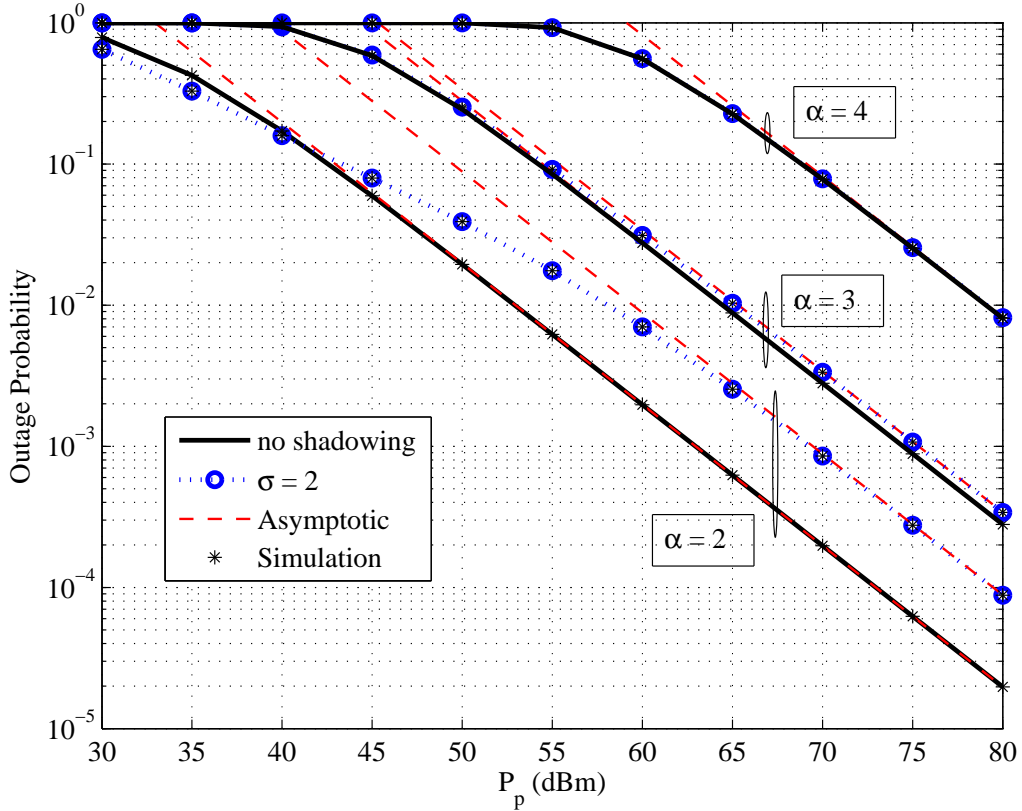


Figure 3.3: The exact and asymptotic outage probability vs the normalized transmit power P_p , for different values of σ and α under $\sigma_n^2 = 0.001$, $\beta = 0.0001$, $P_s = 30\text{dBm}$, $R = 30$, $R_G = 15$, $R_E = 100$, and $\gamma_{Th} = 1$.

for different values of path loss exponents and shadowing. This figure shows that the effect of the shadowing index on environments with different path loss exponents depends on the interferer node density. When the number of interferer nodes increase to very high values, P_{out} approaches 1, while at low interferer node densities, P_{out} is governed primarily by noise. It is interesting to note that at high node densities, the effect of α on the outage probability is minimal.

Fig. 3.5 compares the outage probability when the interferer density β varies, for different values of path loss exponent α and shadowing index σ for $R_G = 25$ and $R_E = 500$. Unlike Fig. 3.4, this figure has a constant primary signal received power, e.g. when power controlling is enabled on the primary system. It can be seen that the effect of the shadowing index on environments with different path loss

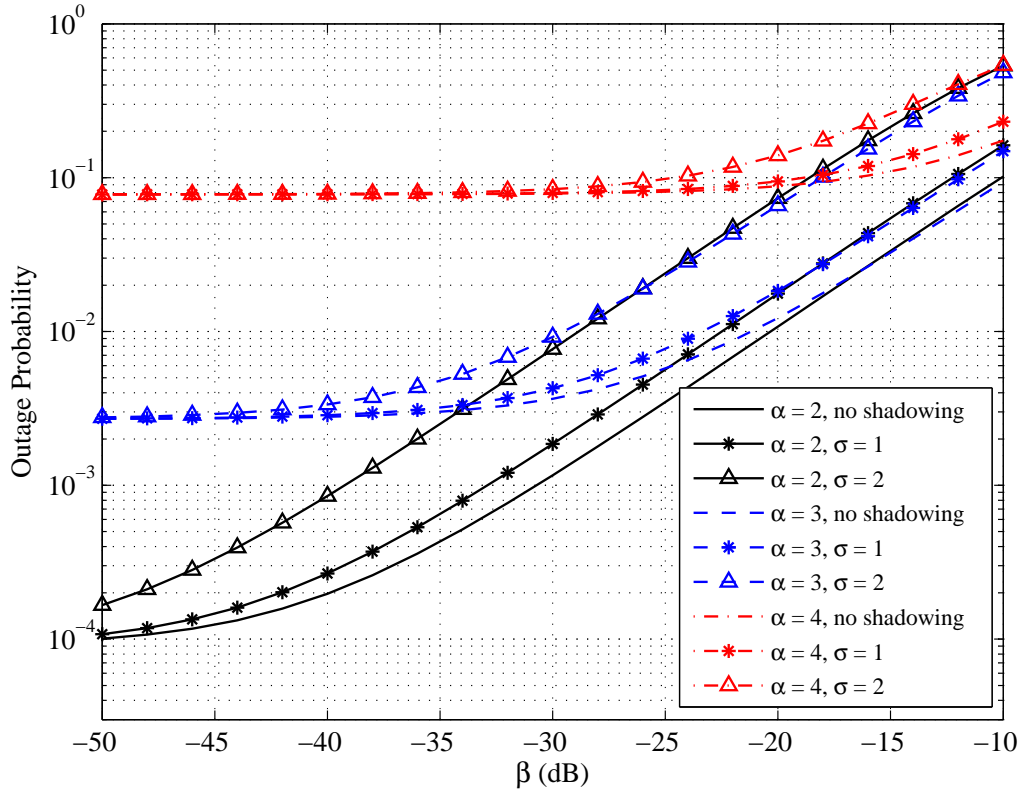


Figure 3.4: The outage probability vs interferer density (β) for different values of σ and α under $P_s = 30$ dBm, $P_p = 70$ dBm, $\sigma_n^2 = 0.001$, $R = 30$, $R_G = 15$, $R_E = 100$, and $\gamma_{Th} = 1$.

exponents depend on the value of interferer node density. For low node densities, the effect of shadowing when the path loss exponent $\alpha = 4$ is lower than that when α equals 2 or 3. When the number of interferer nodes increase to very high values P_{out} approaches 1, while at low node densities, P_{out} is governed primarily by noise.

Fig. 3.6 compares the outage probability with respect to the primary transceiver distance R . In this simulation, we vary R from 10m to 30m such that it lies within the exclusion region, and also within the CR transmitting region. As we can see, the outage probability increases with R , and also increases when the path loss exponent α increases. It can also be observed that at lower α values, the outage for the shadowing index $\sigma = 0$ and $\sigma = 2$ differs considerably. This is not the case at higher path loss exponents. Also, at lower R values, the outage for $\alpha = 2$ and

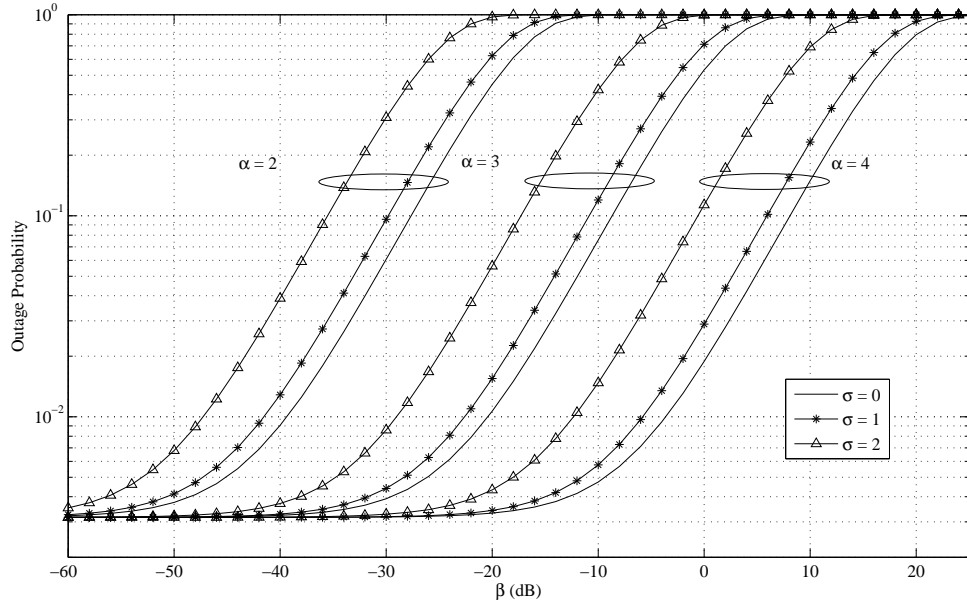


Figure 3.5: The outage probability vs interferer density (β) for different values of σ and α under $P_s = 30$ dBm, $P_p R^{-\alpha} = 25$ dBm, $\sigma_n^2 = 0.001$, $R_G = 25$, $R_E = 500$, and $\gamma_{Th} = 1$.

$\sigma = 2$ almost coincides with $\alpha = 3$ and $\sigma = 0$. Therefore, the effect of shadowing is extremely high at lower path loss exponent values.

3.4.2 Numerical results for the Gamma approximation

Fig. 3.7 shows the CDF of the simulated aggregate interference, and the CDF of the Gamma equivalent aggregate interference. This figure reveals that the aggregate interference roughly follows a skewed alpha-stable distribution [61], where the skewness parameter reduces as β is increased. The two curves show a tight fit for both large and small node density (β) values. Therefore, the Gamma approximation of the aggregate interference is accurate.

Fig. 3.8 depicts the PDF of the approximated aggregate interference for different node densities. As expected, when the node density increases, the average value of the aggregate interference increases and the tails become heavier due to the

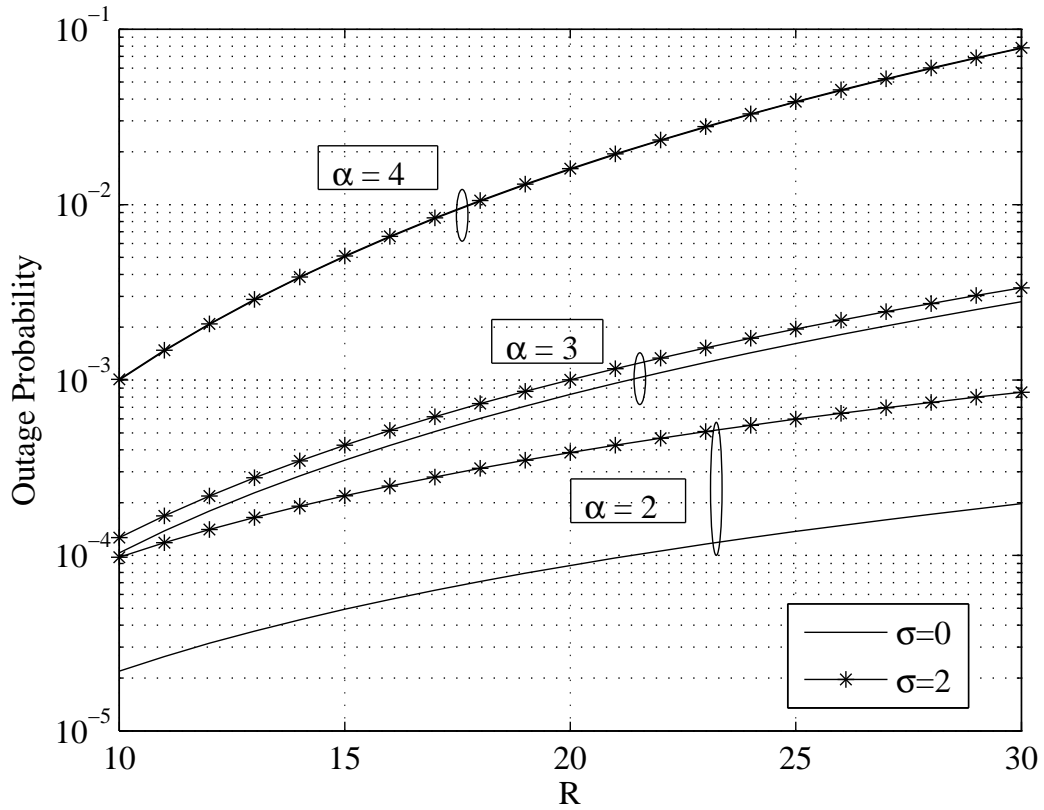


Figure 3.6: The outage probability vs primary transceiver distance (R) for different values of σ and α under $P_s = 30$ dBm, $\gamma_{Th} = 1$, $P_p = 70$ dBm, $R_G = 15$, $R_E = 100$, and $\sigma_n^2 = 0.001$.

increased variance. It is interesting to note that as the node density increases, the PDF becomes more symmetric, and shows a similarity to the Gaussian distribution suggesting that the central limit theorem would be appropriate for use in high node density environments.

In Fig. 3.9, the PDF is plotted when R_G , R_E , and the shadowing variance σ are varied. As σ is increased while keeping the other parameters constant, the PDF flattens out and shows a heavier tail. As the guard distance R_G is increased for fixed shadowing, the interference power reduces as expected, and the PDF is much tighter. Conversely, when R_E is increased while keeping the shadowing index σ constant, the PDF shows a similarity with the Gaussian distribution because many interferer nodes are in the network.

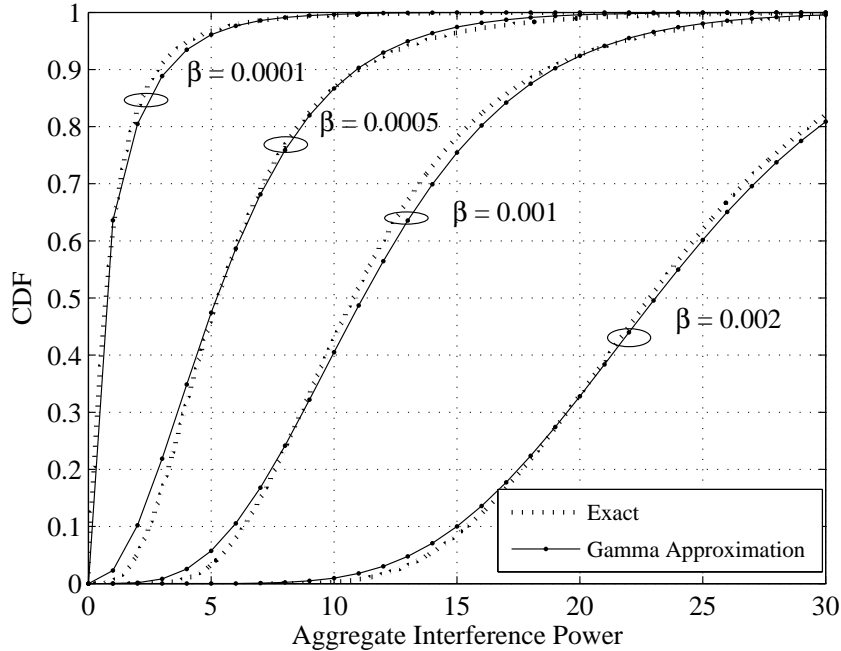


Figure 3.7: The CDF of the aggregate interference and the Gamma approximation for different values of β under $P_s = 30$ dBm, $R_G = 15$, $R_E = 100$, $\alpha = 2$, and no shadowing.

3.5 Conclusion

This chapter investigated the aggregate interference on the primary receiver from interferers for the annular underlay model. A Poisson point process of interferer nodes, a composite fading model with the Generalized- K distribution, and arbitrary path loss exponent values were considered. The exact and approximate MGFs of the aggregate interference, and the exact and asymptotic outage probabilities of the PR were derived. Our numerical results confirmed the analysis and showed that the effect of shadowing is significantly lower with higher path loss exponent values.

The aggregate interference was further modeled as a Gamma random variable. This was necessitated by the mathematical complexity of using the MGF for further analysis. The first two moments of the aggregate interference were derived and matched to the respective moments of a Gamma distribution. This resulted in a simple yet highly accurate approximation of the aggregate interference which in-

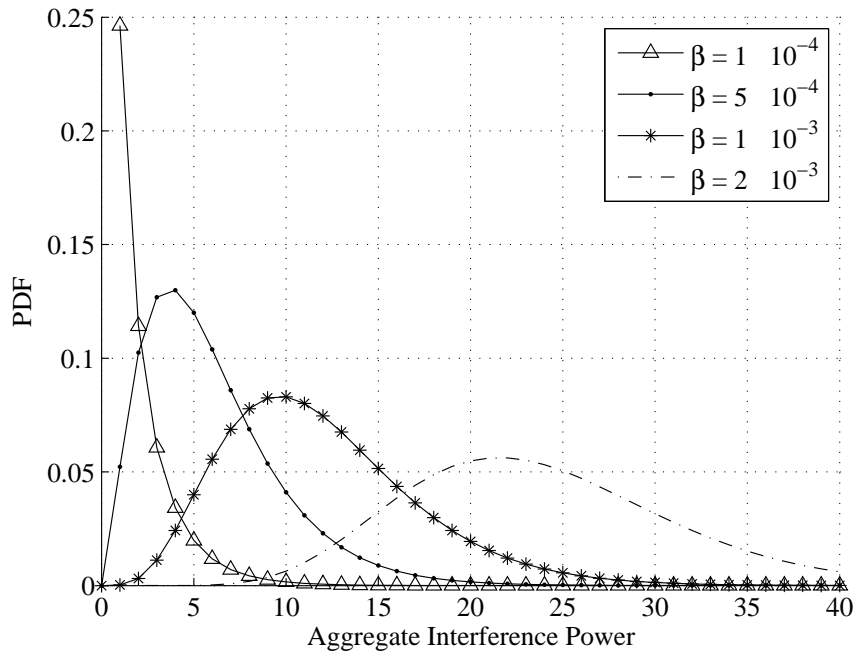


Figure 3.8: The PDF of the Gamma approximated aggregate interference for different values of β under $P_s = 30$ dBm, $R_G = 15$, $R_E = 100$, $\alpha = 2$, and no shadowing.

incorporated all the variable system and channel parameters. The approximation is highly accurate in comparison to the actual distribution for varying node density values.

~

xr

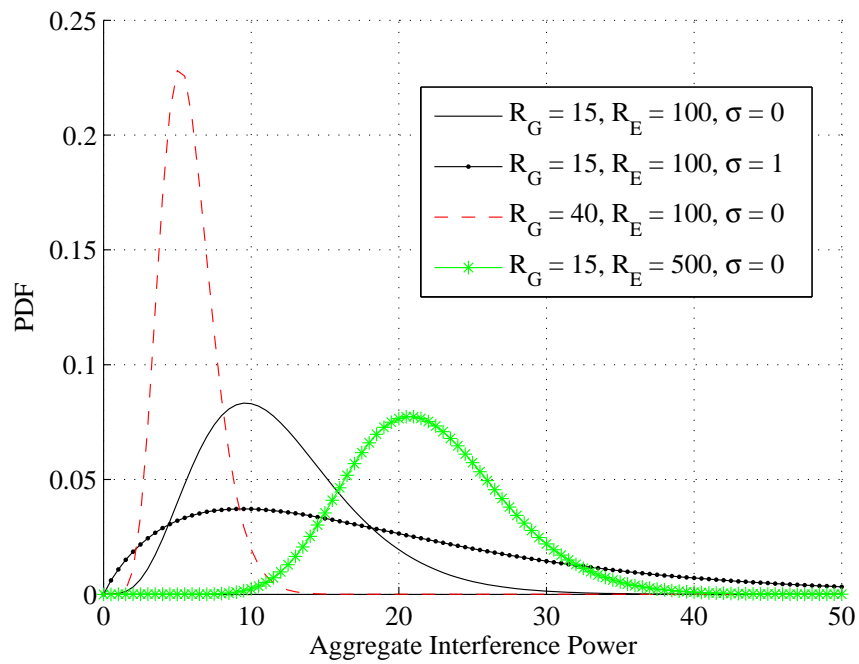


Figure 3.9: The PDF of the Gamma approximated aggregate interference for different values of R_G , R_E , and σ under $P_s = 30$ dBm, $\beta = 1 \times 10^{-3}$, and $\alpha = 2$.

Chapter 4

Approximation models for the aggregate interference

In Chapter 3, an exact analysis and a Gamma approximation to the aggregate interference were developed. This chapter will introduce two more models for the aggregate interference: the multiple-ring model, and the nearest interferer model.

4.1 Introduction

Previously, Chapter 2 introduced the annular underlay model, and Chapter 3 provided an exact analysis and a Gamma approximation to the aggregate interference. This chapter will develop several different models to characterize the aggregate interference which can be used to approximate the annular underlay model, and which are derivatives of that model.

Many approximations and statistical models for the aggregate interference have been widely investigated in literature. For example, [59] proposes a model for the aggregate interference as the sum of normal and log-normal random variables. Reference [59] also obtains an upper bound for the complementary cumulative distribution function (CCDF) of the total interference. In [30], the authors model the aggregate interference when the CR nodes employ power control, contention control, and hybrid power and contention control schemes. The authors fit some of the interference PDFs with log-normal PDFs to reduce complexity. Reference [52] proposes a new statistical model for aggregate interference using cumulants obtained via the application of Campbell's theorem, while [61] shows that when the CR ex-

clusion region around the primary receiver (PR) is zero, the aggregate interference can be accurately modeled as a heavy tailed α -stable distribution. Reference [61] further says that when a significant exclusion region is defined, the tails of the aggregate interference PDFs shorten considerably. Reference [60] investigates the aggregate interference distribution via the central limit theorem. It is shown that interferers in the near field cause the aggregate interference to be a heavy tailed distribution, and in the far field to be a Gaussian distribution. Furthermore, it is shown that the presence of fading reduces the convergence of the aggregate interference to a Gaussian distribution. Moreover, reference [50] presents a statistical model for cognitive radio networks.

This chapter makes two main contributions. First, a new multiple-ring model for the aggregate interference from the annular underlay network is developed. This model is accurate, versatile, and mathematically tractable. Second, a nearest interferer model to approximate the aggregate interference is developed. This model is useful when one particular interfering CR node is more dominant. In some practical situations, this is indeed the case and this analysis will help in developing better interference mitigation procedures. The accuracy of this approximation is evaluated for different parameters.

4.2 A multiple-ring model for underlay interference

4.2.1 Introduction

The annular underlay model in Section 2.3 consists of a Poisson field of cognitive radio (CR) nodes over an annular area with a guard region to reduce interference (Fig. 4.1.a). However, the analysis developed in Chapter 3 is fairly complicated. Therefore, we propose a new model that yields simpler analytical results, and which provides flexibility and versatility to handle different parameters. This model is developed as an approximation of the annular underlay network configuration (Fig. 4.1.a), repeated here for convenience from Section 2.3.

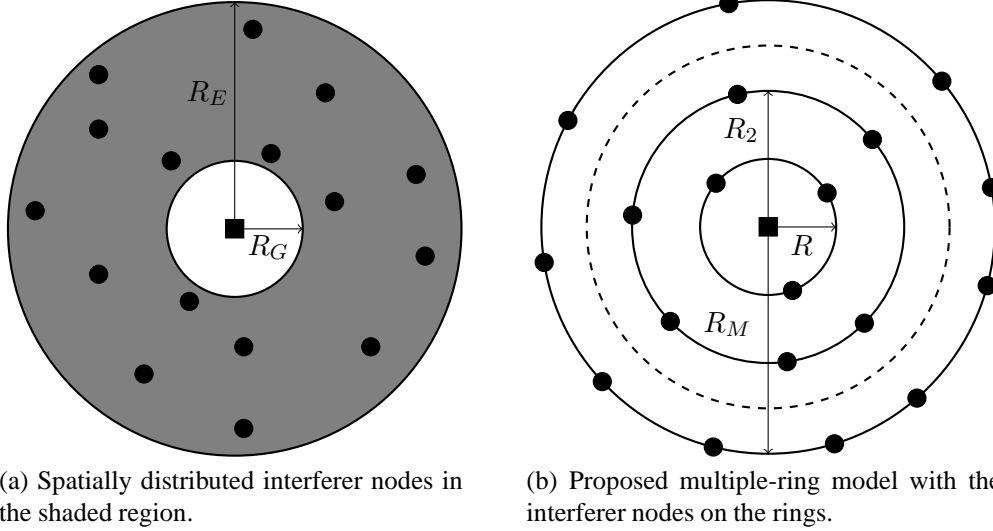


Figure 4.1: System model. Legend: Black circle = interferer nodes, black square = PR, $R_2 = 2R$, and $R_M = MR$.

This new model consists of a set of multiple rings around the PR (Fig. 4.1.b) with a set of interferer nodes on each ring. The system parameters of the new model are chosen to match those of the annular underlay model. The MGF of the aggregate interference for this model will be analyzed under both Rayleigh fading, and composite fading and shadowing. The probability density function (PDF) of the aggregate interference will be obtained for deterministic interferer node numbers, and the exact and asymptotic outage probabilities are derived.

The approximation error of the proposed model is small, and can be further reduced by fine tuning the parameters.

4.2.2 Proposed System Model

The common model for an interferer system is the annular underlay model (Fig. 2.3) discussed in the preceding chapter, with a guard region of radius R_G , and an outer radius of R_E . Usually, $\frac{R_E}{R_G}$ is taken to be between 3 to 20 [49]. For this system, we will develop a new multiple-ring model (Fig. 4.1).

In the proposed model, the interferer nodes are distributed in multiple rings around the PR (Fig. 4.1.b). The radius of the t -th ring is tR , where $t = 1 \dots M$.

For M rings in total, MR is taken for the distance R_E . The radius of the first ring R can be treated as the guard distance R_G . If a smaller value than R_G is used, the guard distance can be taken as the distance to the ν -th ring, νR .

The total number of interferer nodes in a certain ring is modeled as a Poisson random variable arising from a linear Poisson point process. It is independent of the number of interferer nodes in other rings, and the interferer nodes are distributed uniformly on the ring. Let N_k be the number of interferer nodes located on the t -th ring. $P(N_t = n)$ can be written from (2.17) as

$$P(N_t = n) = \frac{(\beta_t 2\pi t R)^n}{n!} e^{-\beta_t 2\pi t R}, \quad n = 0, \dots \quad (4.1)$$

where t is any integer from 1 to M , and β_t is the interferer density of the t -th ring. The density β_t is chosen such that the average number of interferer nodes in the multiple ring model is equal to that of the annular underlay model:

$$\beta(R_E^2 - R_G^2) = \sum_{t=\nu}^M \beta_t 2tR. \quad (4.2)$$

For the considered homogeneous scenario, β_t will not depend on the ring, and will be a constant β_l .

4.2.3 Interference Statistics

To demonstrate the validity of the multiple-ring model, we will next derive the MGF of its aggregate interference. This derivation will consider Rayleigh fading, and combined Rayleigh fading and Gamma shadowing. These MGF expressions are simple, exact, and can be compared against the exact MGF of the annular underlay model (Fig. 4.1.a).

As observed, the average number of interferer nodes in a given ring increases with t . The worst case where all the interferer nodes in the rings are transmitting is assumed. Even if activity factors of the interferer nodes are considered, the distribution can be considered to be that of the active nodes without loss of generality.

The path loss will be modeled to follow the simplified path loss model of (2.16). In our system model, we assume that all the interferer nodes are transmitting at the

same transmit power, and thus, the power level (defined as $P_0 r_0^\alpha$) of each interferer is P_s . The total interference power received at the PR may be written as (2.19)

$$I = \sum_{t=1}^M I_t, \quad (4.3)$$

where I_t is the total interference generated from the interferer nodes of the t -th ring. I_t can be written as

$$I_t = \sum_{l=1}^{N_t} P_s X_{t,l} [tR]^{-\alpha}, \quad (4.4)$$

where X_l is the channel gain corresponding to fading or combined shadowing and fading, for the l -th interferer in the t -th ring. We assume that all the fading and shadowing of the interferer signals are independent of each other, even when they are from the same ring.

If only Rayleigh fading is considered, $X_{t,l}$ can be modeled to follow the exponential distribution (2.5). Similarly, if both Rayleigh fading and Gamma shadowing are considered, $X_{t,l}$ was shown to be modeled as a generalized- K distribution (2.11). In Chapter 2, it was stated that the generalized- K distribution can be approximated by a Gamma distribution as proposed under [29].

Using (4.4) in (4.3), the total interference can be written as

$$I = \sum_{t=1}^M \sum_{l=1}^{N_t} P_s X_{t,l} [tR]^{-\alpha}. \quad (4.5)$$

Let $M_I(s)$ be the MGF of the aggregate interference given by (2.20). Using (4.5), the MGF can be written as

$$\begin{aligned} M_I(s) &= E[e^{-s \sum_{t=1}^M \sum_{l=1}^{N_t} P_s X_{t,l} [tR]^{-\alpha}}] \\ &= E[e^{-s P_s R^{-\alpha} \sum_{t=1}^M t^{-\alpha} \sum_{l=1}^{N_t} X_{t,l}}]. \end{aligned} \quad (4.6)$$

Rayleigh fading

Under Rayleigh fading, all the $X_{t,l}$ values will be independent exponential random variables. Therefore, we can write (4.6) after expanding as

$$M_I(s) = E[E_{X_{1,1}}[e^{-s P_s 1^{-\alpha} R^{-\alpha} X_{1,1}}] \dots E_{X_{1,N_1}}[e^{-s P_s 1^{-\alpha} R^{-\alpha} X_{1,N_1}}] \dots]$$

$$\times E_{X_{M,1}}[e^{-sP_s M^{-\alpha} R^{-\alpha} X_{M,1}}] \dots E_{X_{M,N_M}}[e^{-sP_s M^{-\alpha} R^{-\alpha} X_{M,N_M}}], \quad (4.7)$$

where the first expectation is with respect to $N_1 \dots N_M$. After performing the inner expectations, the MGF becomes

$$\begin{aligned} M_I(s) &= E \left[\frac{1}{(1 + sP_s R^{-\alpha} 1^{-\alpha})^{N_1}} \dots \frac{1}{(1 + sP_s R^{-\alpha} M^{-\alpha})^{N_M}} \right] \\ &= E \left[\prod_{t=1}^M \frac{1}{(1 + sP_s R^{-\alpha} t^{-\alpha})^{N_t}} \right]. \end{aligned} \quad (4.8)$$

Because the number of interferer nodes in the t -th ring is independent of the number of interferer nodes in any other ring, we can write (4.8) as

$$M_I(s) = E_{N_1} \left[\frac{1}{(1 + sP_s R^{-\alpha} 1^{-\alpha})^{N_1}} \right] \dots E_{N_M} \left[\frac{1}{(1 + sP_s R^{-\alpha} M^{-\alpha})^{N_M}} \right]. \quad (4.9)$$

Using (4.1), the expectation with respect to the number of interferer nodes in the t -th ring N_t can be written as

$$\begin{aligned} E_{N_t} \left[\frac{1}{(1 + sP_s R^{-\alpha} t^{-\alpha})^{N_t}} \right] &= \sum_{N_t=0}^{\infty} \frac{1}{(1 + sP_s R^{-\alpha} t^{-\alpha})^{N_t}} \frac{(\beta_l 2\pi t R)^{N_t}}{N_t!} e^{-\beta_l 2\pi t R} \\ &= \sum_{N_t=0}^{\infty} \frac{\left(\frac{\beta_l 2\pi t R}{1 + sP_s R^{-\alpha} t^{-\alpha}} \right)^{N_t}}{N_t!} e^{-\beta_l 2\pi t R} \\ &= e^{\beta_l 2\pi t R \left(\frac{1}{1 + sP_s R^{-\alpha} t^{-\alpha}} - 1 \right)}. \end{aligned} \quad (4.10)$$

Using this result (4.10), (4.9) can be written as

$$\begin{aligned} M_I(s) &= e^{\beta_l 2\pi R \left(\frac{1}{1 + sP_s R^{-\alpha} 1^{-\alpha}} - 1 \right)} e^{\beta_l 2\pi 2R \left(\frac{1}{1 + sP_s R^{-\alpha} 2^{-\alpha}} - 1 \right)} \dots e^{\beta_l 2\pi M R \left(\frac{1}{1 + sP_s R^{-\alpha} M^{-\alpha}} - 1 \right)} \\ &= \prod_{t=1}^M e^{\beta_l 2\pi t R \left(\frac{1}{1 + sP_s R^{-\alpha} t^{-\alpha}} - 1 \right)}, \end{aligned} \quad (4.11)$$

which is the MGF of the aggregate interference.

Composite Rayleigh fading and shadowing

When composite Gamma shadowing and Rayleigh fading are considered, it was shown earlier in the section that $X_{t,l}$ values can be represented by a Gamma PDF.

It is assumed that all the $X_{t,l}$ coefficients are independent. Therefore, similar to Rayleigh fading, we can write $M_I(s)$ as (4.7). After performing the expectations with respect to the $X_{t,l}$ values, $M_I(s)$ becomes

$$\begin{aligned} M_I(s) &= E \left[\frac{1}{(1 + \theta_s P_s R^{-\alpha} 1^{-\alpha})^{kN_1}} \cdots \frac{1}{(1 + \theta_s P_s R^{-\alpha} M^{-\alpha})^{kN_M}} \right] \\ &= E \left[\prod_{t=1}^M \frac{1}{(1 + \theta_s P_s R^{-\alpha} t^{-\alpha})^{kN_t}} \right]. \end{aligned} \quad (4.12)$$

Similar to the case with Rayleigh fading, the number of interferer nodes in the t -th ring is independent of the number of interferer nodes in any other ring. Therefore, the MGF can be written as

$$M_I(s) = E_{N_1} \left[\frac{1}{(1 + \theta_s P_s R^{-\alpha} 1^{-\alpha})^{kN_1}} \right] \cdots E_{N_M} \left[\frac{1}{(1 + \theta_s P_s R^{-\alpha} M^{-\alpha})^{kN_M}} \right] \quad (4.13)$$

Similar to the derivation of (4.10), the expectations with respect to the number of interferer nodes in the rings can be performed. Finally, the MGF of the aggregate interference for Rayleigh fading and Gamma shadowing becomes

$$M_I(s) = \prod_{t=1}^M e^{\beta_t 2\pi t R \left(\frac{1}{(1 + \theta_s P_s R^{-\alpha} t^{-\alpha})^k} - 1 \right)}. \quad (4.14)$$

Extended guard region

When the guard region is extended, the MGF of the aggregate interference is dependent on the rings beyond the ν -th ring ($1 < \nu < M$). Thus, the MGF of the Rayleigh fading scenario becomes

$$M_I(s) = \prod_{t=\nu}^M e^{\beta_t 2\pi t R \left(\frac{1}{(1 + \theta_s P_s R^{-\alpha} t^{-\alpha})^k} - 1 \right)}. \quad (4.15)$$

The MGF of the combined fading and shadowing case is similar.

4.2.4 Suitability as a stand-alone system model

This section will discuss the suitability of the multiple ring model as a stand-alone system model, and the special cases which may occur.

The analysis of the annular underlay network model (Fig. 4.1.a) presents several challenges.

- The incorporation of different transmit powers, path loss exponents, and shadowing variances is complicated.
- Non-homogeneous setups and areas with different CR node densities are difficult to analyze.

The proposed multiple ring model can be used to incorporate these conditions. Moreover, the multiple-ring model may be used to approximate non-annular shapes. For example, interfering nodes over a different polygon region may be approximated.

Differing parameters for interferer nodes

Substituting β_t instead of β_l , α_t instead of α , and P_t instead of P_s , in equations (4.11) and (4.14) will give the desired MGF when the node densities, path loss exponents, and the transmit powers of the interferer nodes are unique. The symbols β_t and P_t denote the node density and transmit power of an interferer in the t -th ring, respectively. Therefore, this multiple-ring system model is extremely versatile to handle general cases. Comparatively, the MGF obtained in the previous chapter for the standard system model is fixed for a particular interferer transmit power and a node density.

Non-random number of interferer nodes

Another special case that can arise is the rings having deterministic interferer node numbers. Therefore, the number of nodes on the t -th ring N_t is not random. In such



Figure 4.2: Linear interferer network. Legend : black dot = interferer nodes, black square = PR.

a scenario, the MGF for the Rayleigh fading case becomes (from 4.8)

$$M_I(s) = \prod_{t=1}^M \frac{1}{(1 + sP_s R^{-\alpha} t^{-\alpha})^{N_t}}. \quad (4.16)$$

The PDF of the aggregate interference is difficult to obtain when N_t is random. But, it can be derived for this special case using the method of [62]. It can be clearly seen that (4.16) is equivalent to the MGF for a sum of Gamma random variables. Therefore, using (2.9) of [62], the PDF of the aggregate interference can be written as

$$f_I(x) = C \sum_{t=0}^{\infty} \frac{\delta_t x^{\rho+t-1} e^{-\frac{x}{P_s R^{-\alpha} M^{-\alpha}}}}{\Gamma(\rho+t) (P_s R^{-\alpha} M^{-\alpha})^{\rho+t}}, \quad x > 0 \quad (4.17)$$

where $\rho = \sum_{t=1}^M N_t$, $C = \prod_{t=1}^M \left(\frac{t}{M}\right)^{\alpha N_t}$, $\delta_{t+1} = \frac{1}{t+1} \sum_{i=1}^{t+1} i \gamma_i \delta_{t+1-i}$, $\delta_0 = 1$, and $\gamma_i = \sum_{t=1}^M \frac{N_t}{i} \left(1 - \left(\frac{t}{M}\right)^{\alpha}\right)^i$. The PDF for the combined Rayleigh fading and shadowing case can be derived similarly.

Approximating interferers in a linear network

To approximate a homogeneous linear interferer network (Fig. 4.2), the guard distance R_G is taken as the distance to the ν -th ring νR , and MR is approximated as R_E . The interferers will be distributed on the rings according to the Poisson point process of (4.1). The density β_t is chosen such that:

$$\beta_{\ln}(R_E - R_G) = \sum_{t=\nu}^M \beta_t \pi t R, \quad (4.18)$$

where β_{\ln} is the interferer density per unit length in the linear interferer network. Unlike the approximation for the homogeneous annular underlay model, β_t values will not be equal. The average number of interferers in each ring will be a constant carrying the form;

$$\beta_t 2\pi t R = C, \quad (4.19)$$

where \mathcal{C} is a constant.

Approximating interferers in a square shaped area

The interfering nodes may be distributed homogeneously in polygon shaped areas. As an example, lets consider a square shaped area (Fig. 4.3). Similar to the previous cases, R_G is taken as the distance to the ν -th ring νR . However, the distance to the M -th ring MR is taken as $\sqrt{2}R_E$. While $tR < R_E$, the interferer density on the t -th ring is a constant, β_t . However, when $R_E < tR < \sqrt{2}R_E$, the interferer density for the t -th ring will be proportional to the percentage of distance that it is within the square. Therefore, the approximation will be as follows;

$$\beta_{sq}(4R_E^2 - \pi R_G^2) = \sum_{t=\nu}^M \beta_t 2\pi tR, \quad (4.20)$$

where β_{sq} is the interferer density of the square region. The values for β_t are,

$$\begin{aligned} \beta_t &= \beta_l, & t < \frac{R_E}{R}, \\ \beta_t &= \left(1 - \frac{8\omega}{2\pi}\right) \beta_l, & \frac{R_E}{R} < t < \frac{\sqrt{2}R_E}{R}, \end{aligned} \quad (4.21)$$

where $\omega = \arccos\left(\frac{R_E}{tR}\right)$ in radians.

4.2.5 Performance analysis

CDF of the SINR

Here, we derive the CDF of the aggregate interference . The SINR γ at the PR can be written as

$$\gamma = \frac{P_p R_{pr}^{-\alpha} Y}{I + \sigma_n^2}, \quad (4.22)$$

where P_p is the power level of the PT, R_{pr} is the distance between the primary transmitter and receiver, σ_n^2 is the noise variance, and Y is the channel gain between the primary transmitter and receiver. Similar to the previous section, due to the mathematical complexity of analyzing for other cases, only the case where the primary

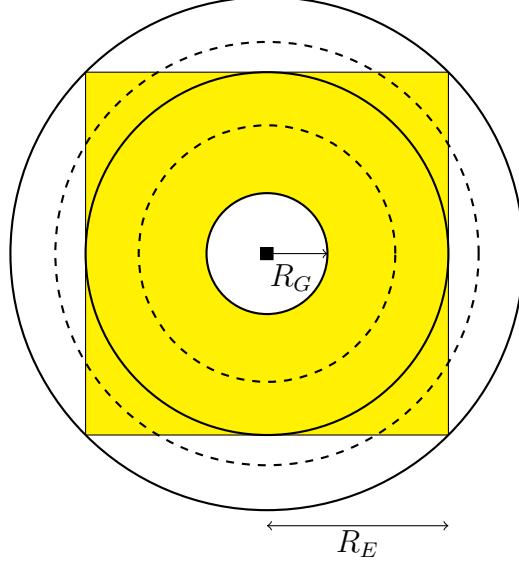


Figure 4.3: Square shaped interferer network. The shaded area contains the interferers. Legend : black square = PR.

signals undergo path loss and Rayleigh fading is considered. Then, Y is a unit exponential PDF given by (2.5), with $\bar{\gamma} = 1$. The variables Y and I are independent. Similar to the derivation of the previous chapter, the CDF of γ is

$$F_{\gamma}(x) = 1 - e^{\left(-\frac{x\sigma_n^2}{P_p R_{pr}^{-\alpha}}\right)} M_I \left(\frac{x}{P_p R_{pr}^{-\alpha}} \right). \quad (4.23)$$

For Rayleigh fading, substituting (4.11) for $M_I(s)$ in (4.23), the CDF of γ becomes,

$$F_{\gamma}(x) = 1 - e^{\left(-\frac{x\sigma_n^2}{P_p R_{pr}^{-\alpha}}\right)} \left(\prod_{t=1}^M e^{\beta_t 2\pi t R \left(\frac{1}{1 + \frac{x}{P_p R_{pr}^{-\alpha}} P_s R^{-\alpha} t^{-\alpha}} - 1 \right)} \right). \quad (4.24)$$

For Rayleigh fading and Gamma shadowing, substituting (4.14) for $M_I(s)$ in (4.23), the CDF of γ becomes,

$$F_{\gamma}(x) = 1 - e^{\left(-\frac{x\sigma_n^2}{P_p R_{pr}^{-\alpha}}\right)} \left(\prod_{t=1}^M e^{\beta_t 2\pi t R \left(\frac{1}{\left(1 + \theta \frac{x}{P_p R_{pr}^{-\alpha}} P_s R^{-\alpha} t^{-\alpha} \right)^k} - 1 \right)} \right). \quad (4.25)$$

Substituting γ_{Th} instead of x gives the outage equation, where γ_{Th} is the threshold SINR level of the PR.

The PDF of the SINR can be found out by differentiating $F_\gamma(x)$ for distinct values of M . But, the PDF for a general M value is extremely complex to obtain.

Asymptotic analysis

The aim in this part of the subsection is to develop an asymptotic equation for the outage probability under Rayleigh fading and both Rayleigh fading and Gamma shadowing, ie. when P_p is considerably larger than P_s , γ_{Th} , and σ_n^2 .

We first consider the Rayleigh fading case. By expanding $e^x = 1 + x + \mathcal{O}(x^2)$ for small x , we obtain

$$e^{\beta_l 2\pi t R \left(\frac{1}{1 + \frac{x}{P_p R_{pr}^{-\alpha} P_s R^{-\alpha} t^{-\alpha}} - 1} \right)} = 1 - (\beta_l 2\pi t R) \frac{P_s R^{-\alpha} t^{-\alpha}}{P_p R_{pr}^{-\alpha}} x + \mathcal{O}(x^2). \quad (4.26)$$

Therefore,

$$\begin{aligned} \prod_{t=1}^M e^{\beta_l 2\pi t R \left(\frac{1}{1 + \frac{x}{P_p R_{pr}^{-\alpha} P_s R^{-\alpha} t^{-\alpha}} - 1} \right)} &\approx \prod_{t=1}^M \left(1 - \beta_l 2\pi t R \frac{P_s R^{-\alpha} t^{-\alpha}}{P_p R_{pr}^{-\alpha}} x \right) \\ &\approx 1 - \left(\beta_l 2\pi R \frac{P_s R^{-\alpha}}{P_p R_{pr}^{-\alpha}} \sum_{t=1}^M t^{1-\alpha} \right) x. \end{aligned} \quad (4.27)$$

Substituting (4.27) in (4.24) and expanding $e^{\left(-\frac{x\sigma_n^2}{P_p R_{pr}^{-\alpha}}\right)}$ via $e^x \approx 1 + x$,

$$\begin{aligned} F_{\gamma_{Asy}}(x) &\approx 1 - \left(1 - \frac{x\sigma_n^2}{P_p R_{pr}^{-\alpha}} \right) \left(1 - \left(\beta_l 2\pi R \frac{P_s R^{-\alpha}}{P_p R_{pr}^{-\alpha}} \sum_{t=1}^M t^{1-\alpha} \right) x \right) \\ &\approx \left(\frac{\sigma_n^2}{P_p R_{pr}^{-\alpha}} + \beta_l 2\pi R \frac{P_s R^{-\alpha}}{P_p R_{pr}^{-\alpha}} \sum_{t=1}^M t^{1-\alpha} \right) x + \mathcal{O}(x^2). \end{aligned} \quad (4.28)$$

Defining $\mathcal{A}_1 = \frac{\sigma_n^2}{P_p R_{pr}^{-\alpha}}$ and $\mathcal{B}_1 = \beta_l 2\pi R \frac{P_s R^{-\alpha}}{P_p R_{pr}^{-\alpha}} \sum_{t=1}^M t^{1-\alpha}$ we get

$$F_{\gamma_{Asy}}(x) = (\mathcal{A}_1 + \mathcal{B}_1) x + \mathcal{O}(x^2), \quad (4.29)$$

which is the asymptotic CDF for the Rayleigh fading scenario.

Similarly, the asymptotic outage for composite Rayleigh fading and Gamma shadowing is given by

$$F_{\gamma_{Asy}}(x) = (\mathcal{A}_2 + \mathcal{B}_2) x + \mathcal{O}(x^2), \quad (4.30)$$

where $\mathcal{A}_2 = \frac{\sigma_n^2}{P_p R_p^{1-\alpha}}$, and $\mathcal{B}_2 = \beta_l 2\pi R \frac{\theta k P_s R^{-\alpha}}{P_p R_p^{1-\alpha}} \sum_{t=1}^M t^{1-\alpha}$.

Moments

The first and second order moments of the aggregate interference are important statistics. The, expected value is found as,

$$\begin{aligned} E[I] &= (-1) \frac{d}{ds} M_I(s)|_{s=0} \\ E[I] &= 2\pi\beta_l R^{1-\alpha} P_s \sqrt{e^{\sigma^2}} \sum_{t=\nu}^M t^{1-\alpha}. \end{aligned} \quad (4.31)$$

The second moment is found as

$$\begin{aligned} E[I^2] &= \frac{d^2}{ds^2} M_I(s)|_{s=0} \\ E[I^2] &= \left(2\pi\beta_l R^{1-\alpha} P_s \sqrt{e^{\sigma^2}} \sum_{t=\nu}^M t^{1-\alpha} \right)^2 + 2\pi\beta_l R^{1-2\alpha} \theta^2 k(k+1) P_s^2 \sum_{t=\nu}^M t^{1-2\alpha} \end{aligned} \quad (4.32)$$

Error statistics

For any new model, it is important to investigate its error statistics. The root mean squared error (RMSE) [63] will be investigated in this regard. If I_{An} and I are the aggregate interference powers of the annular underlay model, and the multiple ring model, the RMSE can be written as $RMSE = \sqrt{MSE}$, where

$$MSE = E[(I_{An} - I)^2]. \quad (4.33)$$

Expanding this, and using (4.31), (4.32), (3.26), and (3.29),

$$\begin{aligned} MSE &= E[I_{An}^2] + E[I^2] - 2E[I_{An}]E[I] \\ &= \left(2\pi\beta_l R^{1-\alpha} P_s \sqrt{e^{\sigma^2}} \sum_{t=\nu}^M t^{1-\alpha} \right)^2 + 2\pi\beta_l R^{1-2\alpha} \theta^2 k(k+1) P_s^2 \sum_{t=\nu}^M t^{1-2\alpha} \\ &\quad + \pi\beta P_s^2 k \theta^2 (1+k) \left(\frac{R_E^{2-2\alpha} - R_G^{2-2\alpha}}{1-\alpha} \right) \end{aligned}$$

$$\begin{aligned}
& + \left(2\pi P_s \beta \sqrt{e^{\sigma^2}} \left(\frac{R_E^{2-\alpha} - R_G^{2-\alpha}}{2-\alpha} \right) \right)^2 \\
& - 2 \left(2\pi \beta_l R^{1-\alpha} P_s \sqrt{e^{\sigma^2}} \sum_{t=\nu}^M t^{1-\alpha} \right) \left(2\pi P_s \beta \sqrt{e^{\sigma^2}} \left(\frac{R_E^{2-\alpha} - R_G^{2-\alpha}}{2-\alpha} \right) \right) \quad (4.34)
\end{aligned}$$

Substituting β_l using (4.2), MR for R_E , and νR for R_G , we obtain

$$\begin{aligned}
MSE &= \pi k(1+k)\theta^2 P_s^2 \beta R^{2-2\alpha} \left(\frac{M^{2-2\alpha} - \nu^{2-2\alpha}}{1-\alpha} + \frac{(M^2 - \nu^2) \sum_{t=\nu}^M t^{1-2\alpha}}{\sum_{t=\nu}^M t} \right) \\
&+ 4\pi^2 k^2 \theta^2 P_s^2 \beta^2 R^{4-2\alpha} \left(\frac{(M^2 - \nu^2)^2 \left(\sum_{t=\nu}^M t^{1-\alpha} \right)^2}{4 \left(\sum_{t=\nu}^M t \right)^2} + \frac{(M^{2-\alpha} - \nu^{2-\alpha})^2}{(2-\alpha)^2} \right. \\
&- \left. \frac{\sum_{t=\nu}^M t^{1-\alpha} (M^2 - \nu^2) (M^{2-\alpha} - \nu^{2-\alpha})}{(2-\alpha) \sum_{t=\nu}^M t} \right). \quad (4.35)
\end{aligned}$$

Coefficient of Variation of the Root Mean Squared Error (CVRMSE)

The coefficient of variation of the root mean squared error is given by

$$CVRMSE = \frac{RMSE}{E[I_{An}]}. \quad (4.36)$$

Normalized error of the mean

The normalized error of the mean (NEM) value is defined as

$$NEM = \frac{|E[I_{An}] - E[I]|}{E[I_{An}]}. \quad (4.37)$$

The $CVRMSE$ and NEM values for different parameter combinations have been tabulated in Table 4.2.5 and Table 4.2.5. While the statistics for the $R = 1, M = 100$ pair are better, the NEM only depends on the path loss exponent value for a given R, M pair. The multiple ring model shows better performance for higher interferer densities, lower path loss exponents, and lower shadowing variances.

	<i>CVRMSE</i>	<i>NEM</i>
$\beta = 0.1, \alpha = 2, \sigma = 0$	0.0654	0.0318
$\beta = 0.1, \alpha = 2, \sigma = 1$	0.0995	0.0318
$\beta = 0.1, \alpha = 3, \sigma = 0$	0.1380	0.1061
$\beta = 0.1, \alpha = 3, \sigma = 1$	0.1800	0.1061
$\beta = 0.01, \alpha = 2, \sigma = 0$	0.1836	0.0318
$\beta = 0.01, \alpha = 2, \sigma = 1$	0.2999	0.0318
$\beta = 0.01, \alpha = 3, \sigma = 0$	0.2984	0.1061
$\beta = 0.01, \alpha = 3, \sigma = 1$	0.4720	0.1061

Table 4.1: Error statistics for $R = 5$ and $M = 20$.

	<i>CVRMSE</i>	<i>NEM</i>
$\beta = 0.1, \alpha = 2, \sigma = 0$	0.0552	0.0062
$\beta = 0.1, \alpha = 2, \sigma = 1$	0.0907	0.0062
$\beta = 0.1, \alpha = 3, \sigma = 0$	0.0831	0.0203
$\beta = 0.1, \alpha = 3, \sigma = 1$	0.1343	0.0203
$\beta = 0.01, \alpha = 2, \sigma = 0$	0.1736	0.0062
$\beta = 0.01, \alpha = 2, \sigma = 1$	0.2861	0.0062
$\beta = 0.01, \alpha = 3, \sigma = 0$	0.2555	0.0203
$\beta = 0.01, \alpha = 3, \sigma = 1$	0.4205	0.0203

Table 4.2: Error statistics for $R = 1$ and $M = 100$.

4.3 Nearest Interferer approximation

4.3.1 Introduction

Until now, several models for the aggregate interference were developed. In Chapter 3, a Gamma model was proposed, while in Section 4.2, a multiple-ring model was developed. This section develops another approximation called the nearest interferer approximation.

With exclusion regions and path loss included, the nearest interferer may dominate the aggregate interference. Furthermore, when there are relatively few interferer nodes (low interferer density), Central Limit Theorem (CLT) based approximations are less accurate. Therefore, characterizing the interference from the nearest node, and analyzing the conditions for its dominance are the focus points of this section. As an intermediate step, the distance distribution of the nearest interferer in the annular underlay network is derived. Moreover, another factor of interest is the impact of power controlling on the aggregate interference.

Very few work has analyzed the spatial distribution of the nearest CR interferer, and the approximation of the aggregate interference with the interference from the nearest node. The works of [64] and [65] have approximated the aggregate interference by that of the nearest node. Reference [64] investigates the trade-off between outage probability and node density, and further studies the effects of interference cancellation. Reference [65] checks the validity of the nearest node approximation and a Gaussian approximation to the aggregate interference. However, none of the prior work do a performance analysis for the nearest node interference using a moment generating function (MGF) based approach. Furthermore, they do not consider any power control schemes used by the interferer nodes. Also, none have compared how the approximation will vary in accuracy as one or more system parameters change.

This section's main objective is to mathematically characterize the interference caused by the nearest interferer, and approximate the aggregate interference with it. In situations where the nearest interferer is more dominant, this analysis will

provide useful insights when designing CR networks. Furthermore, this will help find the situations in which interference cancellation schemes where the dominant interferer is cancelled provide the best results.

The following subsections will evaluate the probability density function (PDF) of the nearest interferer distance, analyze its distribution, and approximate the aggregate interference with the nearest CR interference. Using the approximation, the MGF of the interference is obtained in closed-form for two cases. Namely, where all interferer nodes transmit at a constant power, and where a basic distance based power controlling scheme takes place. A closed-form solution is obtained for the outage probability using the derived MGF. Finally, it will be shown that the nearest CR interference is a lower bound to the aggregate interference which becomes tight as either the interferer density or the distributed area of the interferers decreases, or when the path loss exponent value increases.

4.3.2 System model

The annular underlay network model defined in Fig. 2.3 will be considered. The interferer nodes are assumed to be distributed uniformly in a ring shaped area (Fig. 4.4) with the PR at the center, which has an inner radius R_G , and an outer radius R_E .

The aggregate interference at the PR can be written as (2.19). From the general path loss model (2.16), I_i is expressed as

$$I_i = P_i r_i^{-\alpha} X_i, \quad (4.38)$$

where P_i is the power level (defined as $P_0 r_0^\alpha$) of the i -th interferer, r_i is the distance from the i -th interferer to the PR. When Rayleigh fading is considered, X_i can be written as a unit exponential random variable of the form (2.5). In our model, we consider independent fading of the interfering signals.

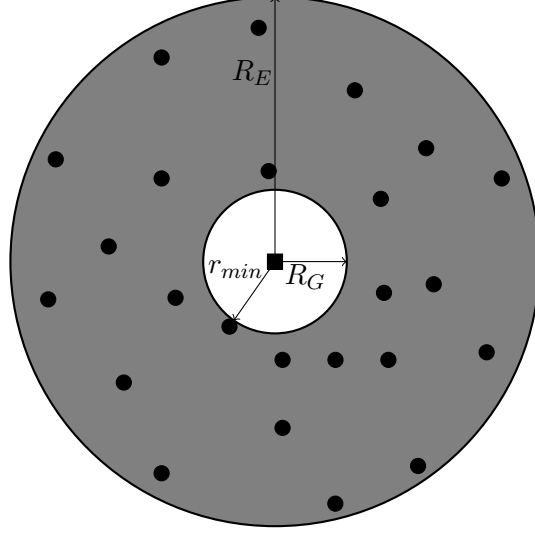


Figure 4.4: System model. Legend: black circle = interferer nodes, black square = PR.

4.3.3 Distribution of the nearest interferer node

Our aim is to approximate the aggregate interference with the interference from the nearest interferer. Therefore, the aggregate interference can be written as

$$I \approx P_{min} r_{min}^{-\alpha} X, \quad (4.39)$$

where P_{min} , r_{min} and X_{min} respectively denote the power level, distance to the PR and the fading coefficient, of the nearest interferer node.

The MGF of the aggregate interference can be obtained from (2.20). In order to evaluate this equation, we need to obtain the PDF of r_{min} , which is defined as

$$r_{min} = \min((r_1, r_2, \dots, r_N)).$$

Using the fact that $\Pr[r_{min} < x]$ implies at least one element of (r_1, r_2, \dots, r_N) is less than x , the CDF of r_{min} given N can be obtained as

$$F_{r_{min}/N}(x) = \Pr[r_{min} < x] = 1 - [\Pr(r_i > x)]^N. \quad (4.40)$$

The PDF of r_i can be expressed as

$$f_R(r_i) = \begin{cases} 2 \frac{\pi r_i}{A_I} & , R_G < r_i < R_E \\ 0 & , \text{otherwise} \end{cases}. \quad (4.41)$$

From (4.41), $Prob(r_i > x)$ can be found out to be $\frac{\pi}{A_I} (R_E^2 - x^2)$. Substituting this in (4.40) and differentiating, we get

$$f_{r_{min}/N}(x) = 2N \left(\frac{\pi}{A_I} \right)^N x (R_E^2 - x^2)^{N-1}. \quad (4.42)$$

Averaging (4.42) with respect to (2.17) for $N \neq 0$, we get

$$\begin{aligned} f_{r_{min}}(x) &= 2x \sum_{N=1}^{\infty} N \left(\frac{\pi}{A_I} \right)^N (R_E^2 - x^2)^{N-1} \frac{(\beta A_I)^N e^{-\beta A_I}}{N!} \\ &= 2\pi\beta e^{-\beta A_I} x \sum_{N=1}^{\infty} \frac{(\pi\beta (R_E^2 - x^2))^{N-1}}{(N-1)!}. \end{aligned} \quad (4.43)$$

With some mathematical manipulations, and substituting for A_I , we can obtain $f_{r_{min}}(x)$ for $N \neq 0$ as

$$f_{r_{min}}(x) = 2\pi\beta x e^{\pi\beta(R_G^2 - x^2)}, R_G < x < R_E. \quad (4.44)$$

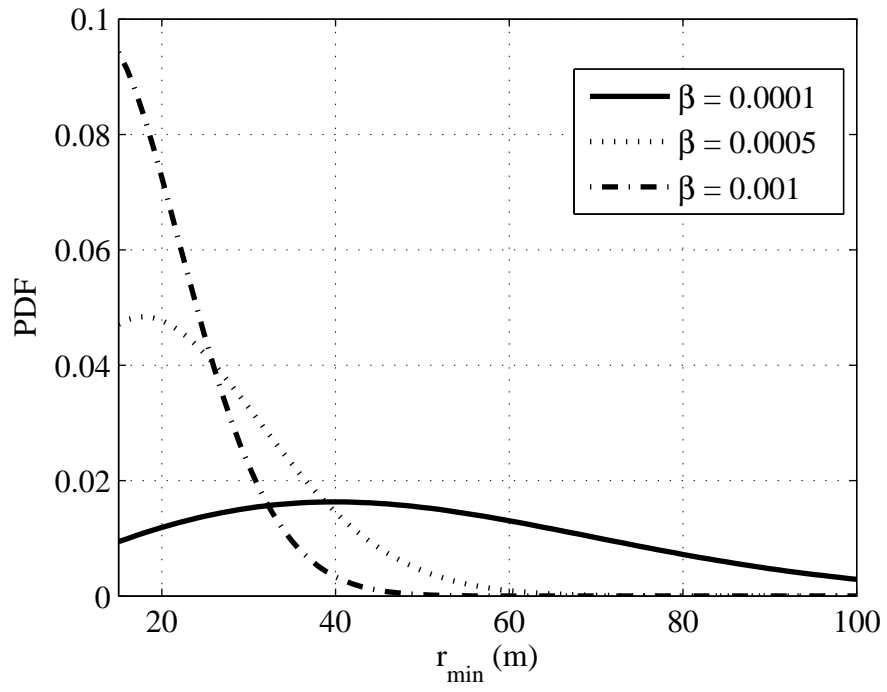
When $N = 0$, $f_{r_{min}}(x)$ is non-existent with probability $e^{-A_I\beta}$.

Fig. 4.5 shows the distribution of $f_{r_{min}}(x)$ under differing β for two R_G values. It is observed that when β is higher, the PDF of $f_{r_{min}}(x)$ shows a sharp drop-off. Conversely, at lower β values, the curves show a more gradual drop with respect to r_{min} . Therefore, it is concluded that at higher β , we can expect a significantly lower value for r_{min} , and thus a higher aggregate interference. At higher R_G , the curves for all β values show increased skewness towards R_G . It is interesting to note that $f_{r_{min}}(x)$ is not dependent on R_E .

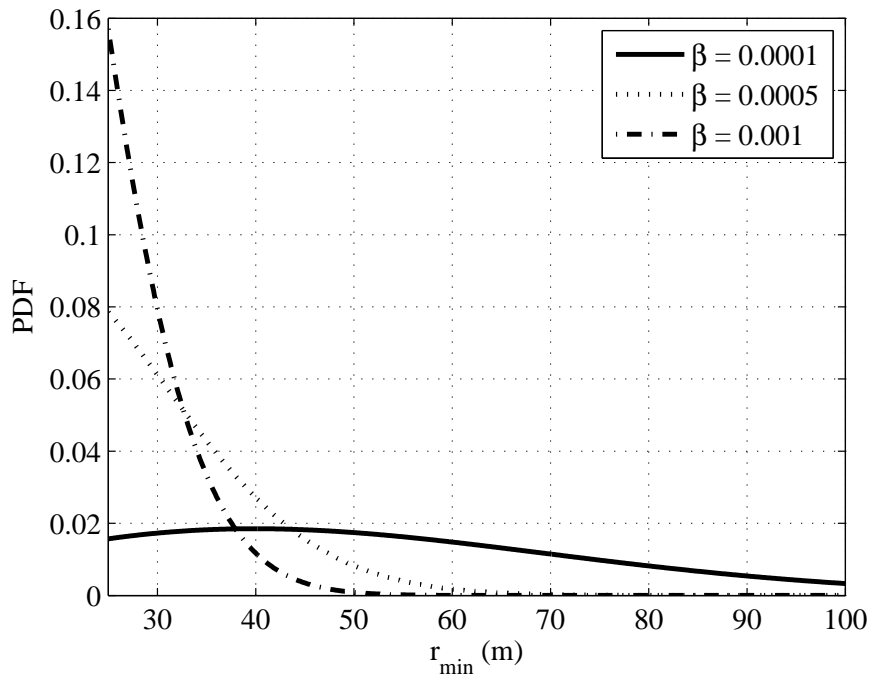
It is more insightful to obtain the PDF of $\frac{r_{min}}{R_G}$. $f_{\frac{r_{min}}{R_G}}(x)$ can be obtained through a simple variable change of (4.44) as

$$f_{\frac{r_{min}}{R_G}}(y) = 2\pi\eta y e^{\pi\eta(1-y^2)}, 1 < y < \frac{R_E}{R_G}, \quad (4.45)$$

where $\eta = \beta R_G^2$. Fig. 4.6 shows the distribution of $f_{\frac{r_{min}}{R_G}}(y)$ when $N \neq 0$ under differing η for $\frac{R_E}{R_G} = 4$. It is observed that when η is higher, the PDF of $f_{r_{min}}(x)$ shows a sharp drop-off. Conversely, at lower η values, the curves show a more gradual drop with respect to $\frac{r_{min}}{R_G}$. When η gets significantly low, $f_{\frac{r_{min}}{R_G}}(y)$ does not drop off with respect to $\frac{R_E}{R_G}$, and increases. Therefore, it is concluded that at higher



(a) $R_G = 15m$



(b) $R_G = 25m$

Figure 4.5: $f_{r_{min}}(x)$ for varying β values when $N \neq 0$

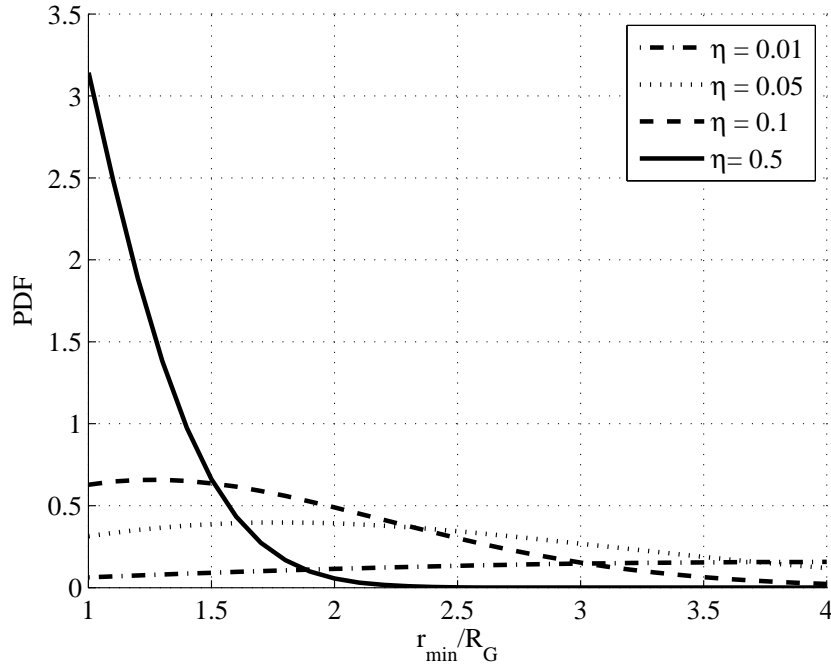


Figure 4.6: $f_{\frac{r_{min}}{R_G}}(y)$ for varying η values when $N \neq 0$, $\frac{R_E}{R_G} = 4$.

η , we can expect a significantly lower value for $\frac{r_{min}}{R_G}$, and thus a higher aggregate interference. It is interesting to note that the shapes of the curves are not dependent on $\frac{R_E}{R_G}$.

We can observe that the nearest interferer terminal would have a much higher effect on the PR's aggregate interference when η is lower. Moreover, in practice, when designing a CR system at higher η values, increasing the inner radius instead of reducing the node density is a more effective technique to ensure a guaranteed PR performance while maximizing the amount of CR nodes employed.

4.3.4 Derivation of the MGF

In the following subsections, we will derive the MGF of the aggregate interference when the CR nodes employ constant transmit power and when the CR nodes employ a distance based power control scheme.

Constant power interferer nodes

When the power levels of each interferer is constant, and not dependent on distance, (2.20) can be written as

$$M_I(s) = E_{X,r_{min}}[e^{-sI}] = E_{r_{min}}[E_X[e^{-sP_s r_{min}^{-\alpha} X}]], \quad (4.46)$$

where P_s is the constant power of a interferer. Averaging with respect to X , we find

$$M_I(s) = E_{r_{min}} \left[\frac{1}{1 + P_s s r_{min}^{-\alpha}} \right]. \quad (4.47)$$

When $P_s s r_{min}^{-\alpha} < 1$, we can expand (4.47) as an infinite series, and get

$$M_I(s) = E_{r_{min}} \left[\sum_{t=0}^{\infty} (-P_s s r_{min}^{-\alpha})^t \right]. \quad (4.48)$$

For most practical values of system parameters, the summation will converge. Using (4.44) and averaging (4.48), we obtain the MGF as,

$$\begin{aligned} M_I(s) &= e^{-A_I \beta} + \pi \beta e^{\pi \beta R_G^2} \\ &\times \sum_{t=0}^{\infty} \left((-P_s s)^t \left(\frac{E_{\frac{t\alpha}{2}}(\pi \beta R_G^2)}{R_G^{t\alpha-2}} - \frac{E_{\frac{t\alpha}{2}}(\pi \beta R_E^2)}{R_E^{t\alpha-2}} \right) \right). \end{aligned} \quad (4.49)$$

The exact MGF can be obtained similar to the derivation of (3.12) as

$$M_I^{exact}(s) = e^{\beta A_I (M_I^i(s) - 1)}, \quad (4.50)$$

where $M_I^i(s)$ is the MGF of the interference from a single interferer, given by

$$M_I^i(s) = E[e^{-sP_s r_i X_i}]. \quad (4.51)$$

The PDF of r_i is given by (4.41), and the PDF of X_i is given by (2.5). Averaging with respect to these gives the result

$$M_I^i(s) = \frac{\pi}{A_I} \left(R_G^2 \left(\mathcal{W}\left(\frac{R_G^\alpha}{P_s s}\right) - 1 \right) - R_E^2 \left(\mathcal{W}\left(\frac{R_E^\alpha}{P_s s}\right) - 1 \right) \right), \quad (4.52)$$

where $\mathcal{W}(x) = {}_2\mathcal{F}_1(1, 2/\alpha; 1 + 2/\alpha; -x)$.

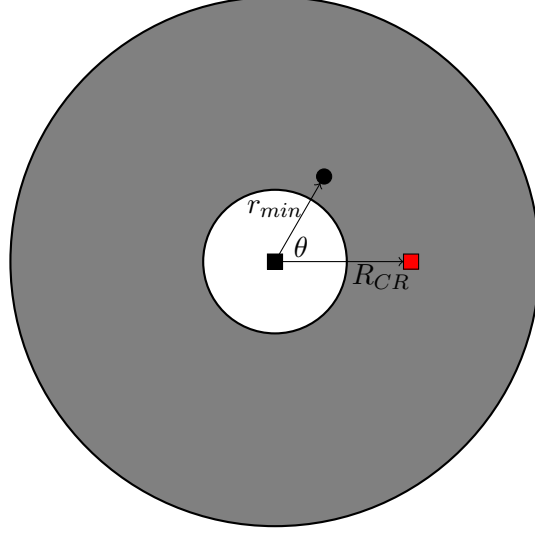


Figure 4.7: System model for a CR setup employing power control. Legend: black circle = nearest interferer node, black square = PR, red square = CR receiver.

interferer nodes employing power control

In this subsection, we consider a distance dependent power control scheme [30] [66] where the interferer nodes control their power in order to ensure a constant average received power level to a single CR receiver. A practical example for such a scenario would be wireless sensor nodes transmitting information to their base station.

Without loss of generality, we can take the PR to be located at the origin and the CR receiver be located a distance R_{CR} from the PR along the x -axis (Fig. 4.7). Let θ be the angle from the positive x -axis to the nearest CR transmitter. We assume θ to be uniformly distributed between 0 and 2π . Let P_{rec} be the average power level ensured at the CR receiver. R_{CR} is assumed to be a constant in the analysis. But, if required, it can be modeled as a random variable. The average transmit power of the nearest interferer can be written as

$$P_{min} = P_{rec} (r_{min}^2 + R_{CR}^2 - 2r_{min}R_{CR}\cos\theta)^{\frac{\alpha}{2}}. \quad (4.53)$$

Let I_{PC} be the interference from the nearest interferer node when the power control scheme takes place. The the MGF $M_{I_{PC}}(s)$ of this can be written as

$$M_{I_{PC}}(s) = E_{\theta}[E_{r_{min}}[E_X[e^{-sP_{min}r_{min}^{-\alpha}X}]]]. \quad (4.54)$$

Substituting for P_{min} and carrying ou the expectation with respect to X , (4.54) becomes,

$$M_{IPC}(s) = E_{\theta} \left[E_{r_{min}} \left[\frac{1}{1 + sP_{min}r_{min}^{-\alpha}} \right] \right]. \quad (4.55)$$

After performing a series expansion, (4.55) becomes,

$$M_{IPC}(s) = \sum_{t=0}^{\infty} (-sP_{rec})^t \times E_{\theta} \left[E_{r_{min}} \left[r_{min}^{-\alpha t} (r_{min}^2 + R_{CR}^2 - 2r_{min}R_{CR}\cos\theta)^{\frac{\alpha t}{2}} \right] \right]. \quad (4.56)$$

When α is an even number, we can simplify (4.56) using the binomial expansion and obtain the following equation for $M_{I_{app}}^{PC}(s)$ after averaging with respect to θ and r_{min} :

$$M_{IPC}(s) = e^{-A_I\beta} + 2\pi^2\beta e^{\pi\beta R_G^2} \sum_{t=0}^{\infty} (-P_{rec}s)^t \sum_{k=0}^{\frac{\alpha t}{2}} \binom{\frac{\alpha t}{2}}{k} \sum_{l=0}^{\lfloor \frac{k}{2} \rfloor} \binom{k}{2l} \times R_{CR}^{2k-2l} \frac{(4l-1)!!}{(2l)!} \left(\frac{E_{k-l}(\pi\beta R_G^2)}{R_G^{2k-2l-2}} - \frac{E_{k-l}(\pi\beta R_E^2)}{R_E^{2k-2l-2}} \right), \quad (4.57)$$

where $\lfloor x \rfloor$ denotes the largest integer less than x . The convergence of (4.56) is relatively lower compared to (4.49). In the case that R_{CR} is a random variable, further averaging needs to be done on (4.57).

4.3.5 Moments

Moments of the nearest nodes' interference may be important when cconducting further research on the approximation. Specially, the first and second moments are highly important.

Constant power interferer nodes

The general n^{th} order moment of the interference from the nearest node can be obtained from (4.49) as

$$E[I^n] = (-1)^n \frac{d^n}{ds^n} M_I(s) \Big|_{s=0}$$

$$= n! \pi \beta P_s^n (-1)^n e^{\pi \beta R_G^2} \left(\frac{E_{\frac{\alpha}{2}}(\pi \beta R_G^2)}{R_G^{\alpha-2}} - \frac{E_{\frac{\alpha}{2}}(\pi \beta R_E^2)}{R_E^{\alpha-2}} \right). \quad (4.58)$$

interferer nodes employing power control

Similar to above, the general n^{th} order moment for the power controlling scenario is obtained from (4.57) as

$$\begin{aligned} E[I_{PC}^n] &= 2n! \pi^2 \beta P_{rec}^n (-1)^n e^{\pi \beta R_G^2} \sum_{t=0}^{\infty} (-P_{rec} s)^t \sum_{k=0}^{\frac{\alpha t}{2}} \binom{\frac{\alpha t}{2}}{k} \sum_{l=0}^{\lfloor \frac{k}{2} \rfloor} \binom{k}{2l} \\ &\times R_{CR}^{2k-2l} \frac{(4l-1)!!}{(2l)!} \left(\frac{E_{k-l}(\pi \beta R_G^2)}{R_G^{2k-2l-2}} - \frac{E_{k-l}(\pi \beta R_E^2)}{R_E^{2k-2l-2}} \right). \end{aligned} \quad (4.59)$$

4.3.6 Outage Analysis

In this section, the outage probability at the PR will be derived. The signal to interference and noise ratio (γ) at the PR is denoted similar to the previous section. The CDF of γ can be obtained as

$$F_{\gamma}(x) = 1 - e^{\left(-\frac{x \sigma_n^2}{P_p R^{-\alpha}}\right)} M_I \left(\frac{x}{P_p R^{-\alpha}} \right). \quad (4.60)$$

For the constant transmit power interferer nodes, $F_{\gamma}(x)$ becomes

$$\begin{aligned} F_{\gamma}(x) &= 1 - e^{\left(-A_I \beta + \frac{x \sigma_n^2}{P_p R^{-\alpha}}\right)} - \pi \beta e^{\left(\pi \beta R_G^2 - \frac{x \sigma_n^2}{P_p R^{-\alpha}}\right)} \\ &\times \sum_{t=0}^{\infty} \left(\left(-\frac{P_s x}{P_p R^{-\alpha}} \right)^t \left(\frac{E_{t\frac{\alpha}{2}}(\pi \beta R_G^2)}{R_G^{t\alpha-2}} - \frac{E_{t\frac{\alpha}{2}}(\pi \beta R_E^2)}{R_E^{t\alpha-2}} \right) \right). \end{aligned} \quad (4.61)$$

For interferer nodes employing power control (4.3.4), $F_{\gamma}(x)$ becomes

$$\begin{aligned} F_{\gamma}^{PC}(x) &= 1 - e^{\left(-A_I \beta + \frac{x \sigma_n^2}{P_p R^{-\alpha}}\right)} \\ &- 2\pi^2 \beta e^{\left(\pi \beta R_G^2 - \frac{x \sigma_n^2}{P_p R^{-\alpha}}\right)} \sum_{t=0}^{\infty} \left(-\frac{P_{rec} x}{P_p R^{-\alpha}} \right)^t \sum_{k=0}^{\frac{\alpha t}{2}} \binom{\frac{\alpha t}{2}}{k} \sum_{l=0}^{\lfloor \frac{k}{2} \rfloor} \binom{k}{2l} \\ &\times R_{CR}^{2k-2l} \frac{(4l-1)!!}{(2l)!} \left(\frac{E_{k-l}(\pi \beta R_G^2)}{R_G^{2k-2l-2}} - \frac{E_{k-l}(\pi \beta R_E^2)}{R_E^{2k-2l-2}} \right). \end{aligned} \quad (4.62)$$

Substituting the threshold level γ_{Th} for x gives us the outage probability.

4.4 Numerical Results

In this section a comparison is done between simulation results and the theoretical equations in order to assess their accuracy. Furthermore, performance trends due to parameter changes will be examined.

4.4.1 Numerical results of the multiple-ring model

This section shows the accuracy and performance of the multiple-ring model. The exact and asymptotic variation of the outage probability with P_p is shown. Simulations are performed for both shadowing and non-shadowing environments to confirm our theoretical results. Moreover, comparisons between the multiple-ring model and the annular underlay model are performed. The following parameter values will be used: noise variance $\sigma_n^2 = 0.001$, interferer node power level $P_s = 30$ dBm, $\gamma_{Th} = 1$ and $R_{pr} = 30$ for all the plots for comparison purposes.

It is necessary to establish the accuracy of the multiple-ring model for varying path loss exponent (α) and shadowing levels (σ). In Fig. 4.8, the theoretical results match perfectly with the simulations, and as P_p increases, the asymptotic curves coincide with the exact curves. When the path loss exponent increases, shadowing has little affect on the outage. But, for free space propagation ($\alpha = 2$), the shadowing effects are substantial, and the curve for $\sigma = 2$ under $\alpha = 2$ has worse performance than the curve for Rayleigh fading under $\alpha = 3$. For the chosen R_{pr} , the outage increases with α , but this may not be the case if R_{pr} had been significantly smaller than R .

We now compare our proposed model (Fig. 4.1.b) with the annular underlay model (Fig. 4.1.a) in Fig. 4.9. We simply consider all rings with equal density such that $\beta_l = 0.01$. Then, the equivalent node density in the annular underlay model is 6.25×10^{-4} . For these curves, the outage probabilities are virtually identical for higher path loss exponent values, and extremely close under free space propagation, while shadowing doesn't seem to affect the accuracy of the outage significantly.

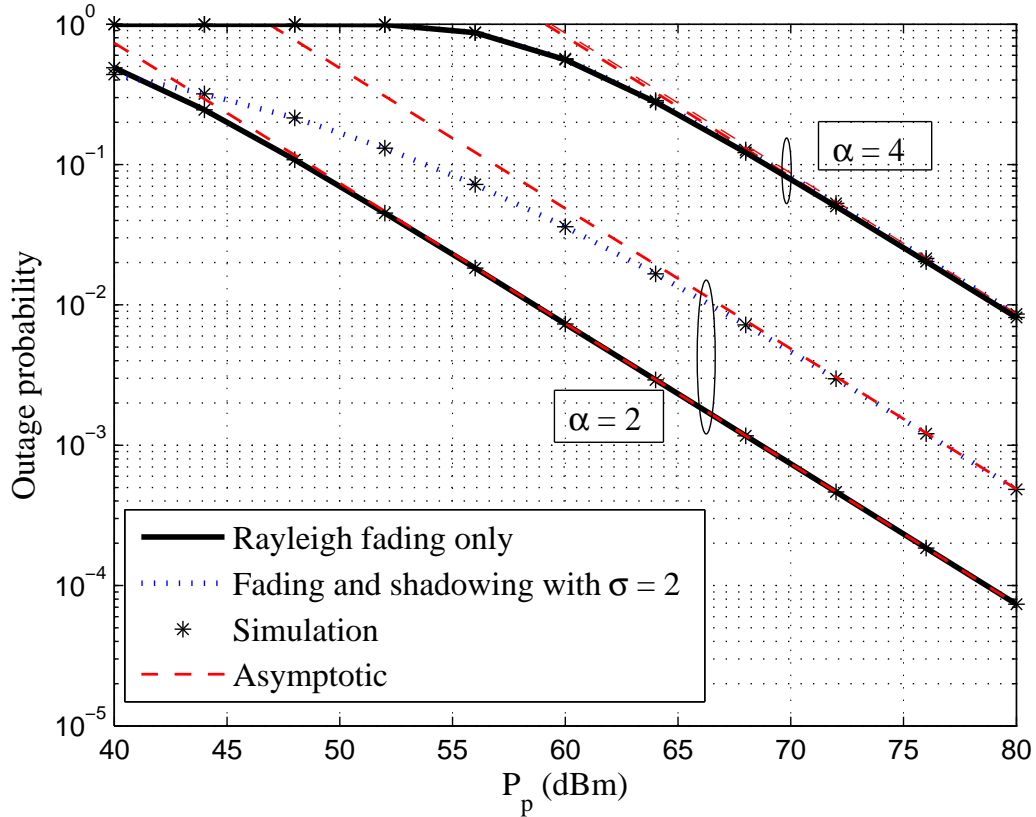


Figure 4.8: The exact and asymptotic outage probability vs the primary system power level P_p , for different values of σ and α under $\beta_l = 0.01$, $R = 20$, and $M = 5$.

However, as was shown before, the error statistics of the model deteriorates when shadowing is present. The perceived increase in accuracy of the outage at higher path loss exponents is mainly due to the affects of noise.

It is important to calculate the error of the proposed model, and to observe how the error changes as a function of ring radii. In Fig. 4.10, the percentage error of the multiple-ring model is compared for different R and M values. The parameters for the annular underlay model are $\beta = 0.001$, a guard distance of 20, and the outer distance of 100. R and M pairs of (20,5), (10,10), and (5,20) are used for comparisons. The node density β_l for each case will be 0.016, 0.008889, and 0.004706 respectively. For $R = 10$, t is taken from 2 to M , and for $R = 5$, t is taken from 4 to M . The percentage error reduces with R . With respect to P_p , the

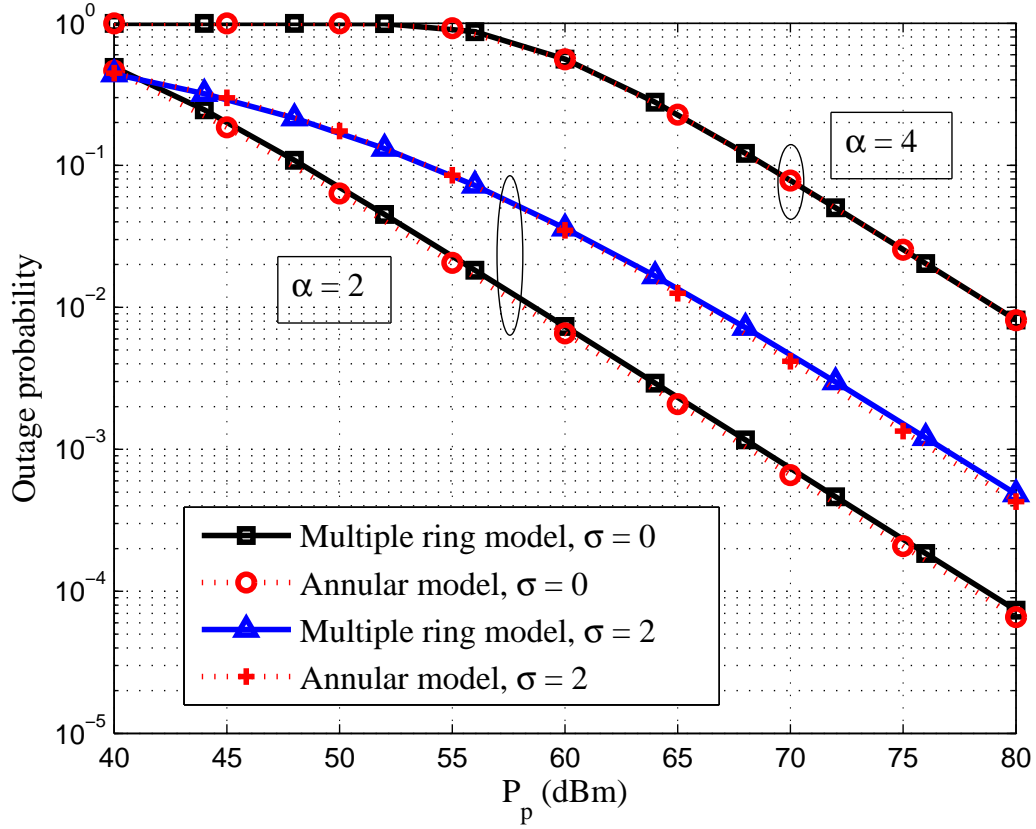


Figure 4.9: Comparison of the outage probability vs primary system power level P_p with different values of σ and α , for the multiple-ring model and the annular underlay model under $\beta_l = 0.01$, $R = 20$, and $M = 5$. The values for β , R_G and R_E have been chosen accordingly.

percentage errors for all 3 cases rise up to a certain level, and then keeps constant.

Furthermore, it is necessary to compare the performance of the proposed model under varying CR node densities. In Fig. 4.11, the outage for the proposed system model is almost identical to the annular underlay model. Moreover, there is no increase of error as the interferer node density β increases. The approximation error probability under $P_p = 60$ dBm is 2.9% for $\beta = 0.001$, 2.9% for $\beta = 0.01$, and 1.9% for $\beta = 0.1$.

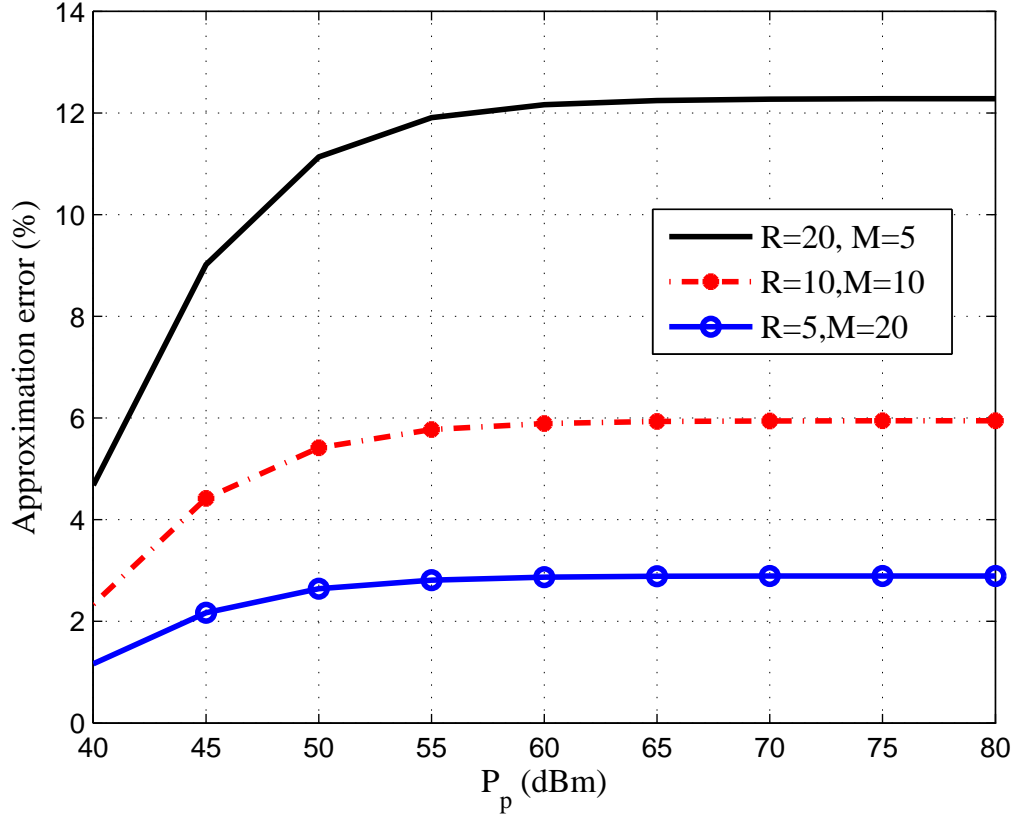


Figure 4.10: The error percentage of the outage of the multiple-ring model vs the primary system power level P_p , for different values of M and R under $\beta = 0.001$, $\alpha = 2$, and $\sigma = 0$. The value of β_l has been chosen appropriately for each case.

4.4.2 Numerical results for the nearest interferer approximation

In this subsection, we show the behaviour of the exact outage probability, and the nearest interferer approximation with respect to changing the primary power level P_p and the guard distance R_G , for different conditions, and obtain insights into the situations where the nearest interferer approximation is applicable.

The outage with respect to the primary transmit power level P_p for the scenario when interferer nodes employ basic power control is plotted in Fig. 4.12. We conclude that the approximation is very tight for low P_{rec} values. When R_{CR} increases, the outage probability increases correspondingly because of the need to transmit at a higher power, and the approximation diverges from the exact value. Thus, although

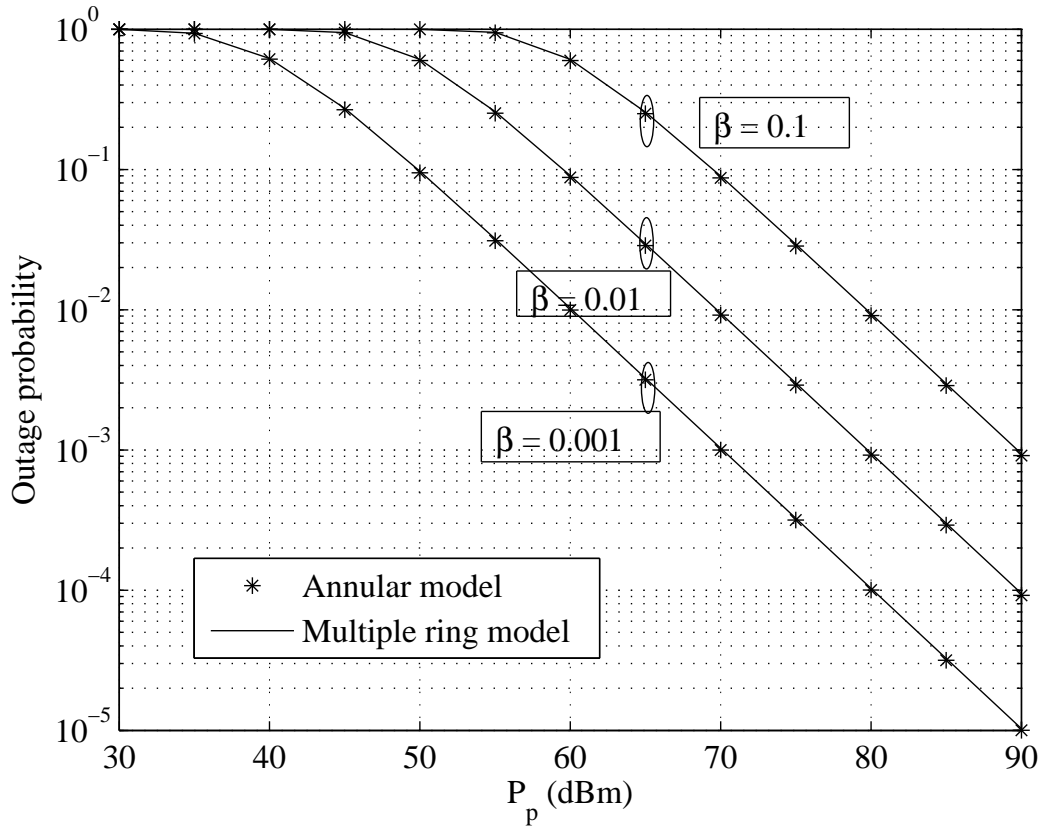


Figure 4.11: The outage probability vs the primary system power level P_p , under different values of β , for the annular underlay model and the multiple-ring model. $\alpha = 2$, $\sigma = 0$, $R = 5$, and $M = 20$.

the approximation shows a tight match when $R_{CR} = 0$, it shows a significant variation at $R_{CR} = 275$. The rest of this section will compare the performance of the constant powered CR case.

Fig. 4.13 compares the outage probability of constant powered interferer nodes under different primary transceiver distance R values. As R increases, the outage probability increases significantly. This is because, when R increases, the primary signal power diminishes and the interference power has a more significant effect on the receiver. But, it is interesting to note that R does not have any bearing on the error between the exact outage probability and the approximation. In addition, Fig. 4.13 compares the theoretical values of the outage probability to the ones obtained through Monte-Carlo simulations. We see that the simulations and theory match

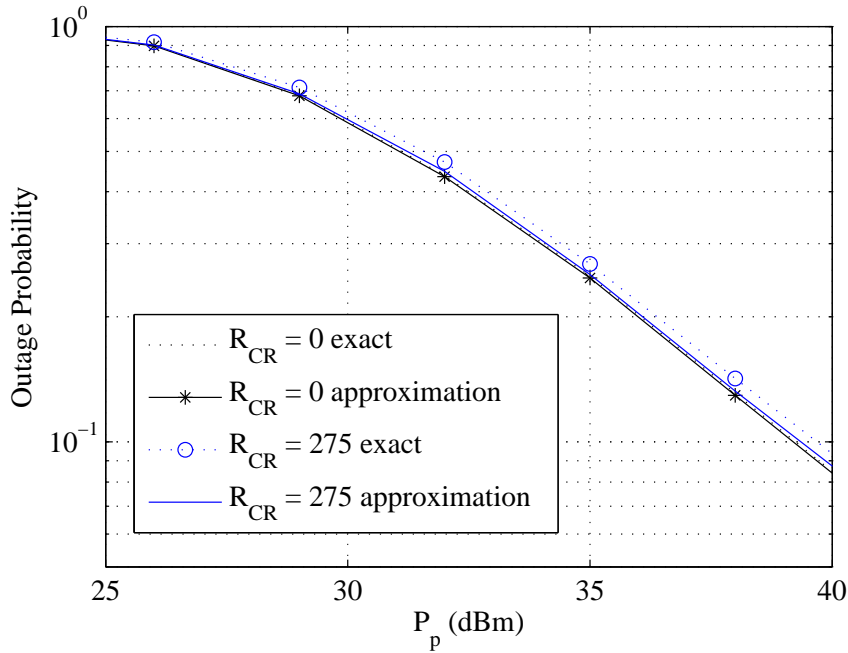


Figure 4.12: Outage probability vs P_s for power controlled interferer nodes under $R_{CR} = 0$ and $R_{CR} = 275$ for $\beta = 0.0001$, $\alpha = 2$, $R_E = 200$, $R_G = 25$, $R = 30$, $P_{rec} = -30$ dBm, $\gamma_{Th} = 1$, and $\sigma_n^2 = 0.001$.

well.

Fig. 4.14 shows the variation of the outage probability with respect to the guard distance R_G , under three different node density β values. It is observed that at higher R_G , the exact outage probability, and the outage given by the nearest interferer approximation converge. This is because the average number of interferer nodes reduces as R_G is increased and therefore, the nearest interferer is more dominant. In addition, we see that the accuracy of the approximation depends on the interferer density. At lower β values, the approximation is a close to the outage probability, while at higher β , the two curves are more divergent. AS R_G is increased further, the performance of the PR is mainly inhibited by noise due to the interference power reducing due to path loss. Therefore, the curves flatten out.

In Fig. 4.15, we plot the variation of the outage probability with respect to the interferer power level P_s . It is seen that when the path loss exponent α is high, the approximation is extremely accurate to the actual aggregate interference. This

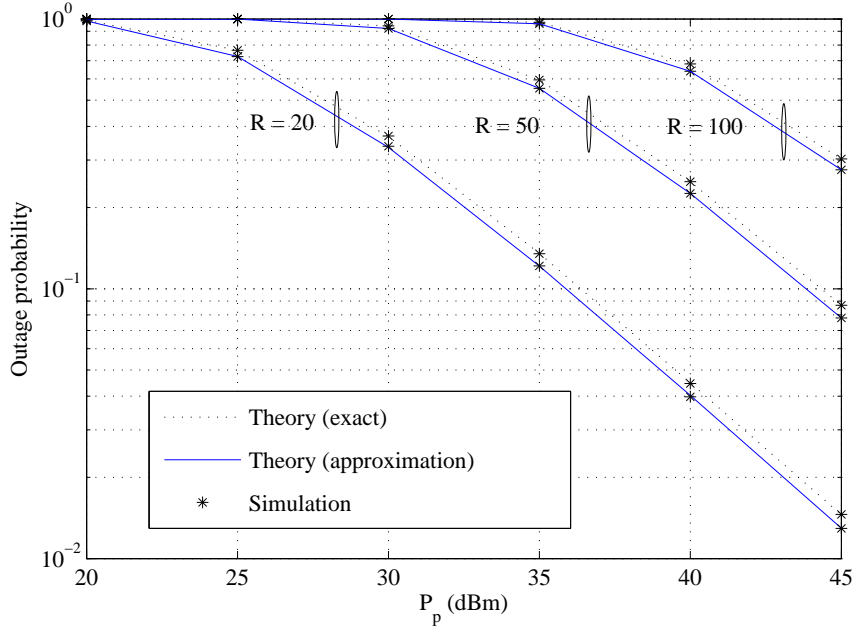


Figure 4.13: Outage probability vs P_p for different values of R , with $R_E = 500$, $R_G = 50$, $P_s = 20$ dBm, $\beta = 0.0001$, $\alpha = 2$, $\gamma_{Th} = 1$, and $\sigma_n^2 = 0.001$.

is because at higher path loss factors, the interference is dominated by the nearest interferer. In many practical wireless channels such as in dense urban environments or hilly terrain, α is particularly high and the nearest interferer approximation is extremely valid. For a path loss exponent value of 2 (free space propagation), when P_s is low, the aggregate interference can be validly approximated by the interference from the nearest interferer. Even when P_s is increased for free space propagation, the error is minimal and when we reduce β , the error gets further reduced.

Therefore, the nearest interferer approximation is reasonably accurate under several conditions. These include high path loss exponent values, lower interferer node densities, and higher guard distances (R_G).

4.5 Conclusion

This chapter included 1) a new multiple-ring model to analyze the aggregate interference, and 2) the nearest interferer approximation to the aggregate interference.

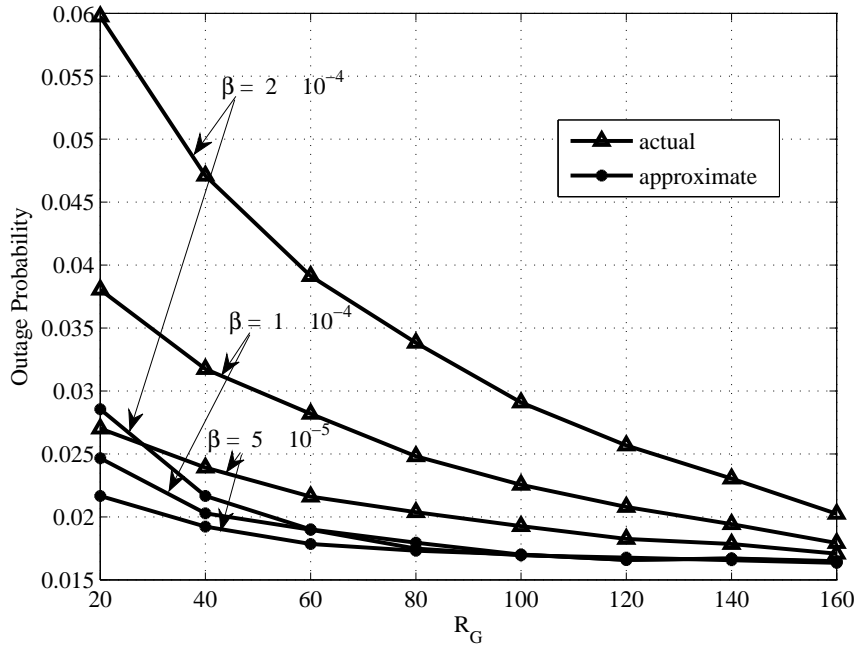


Figure 4.14: Outage probability vs R_G for different values of β , with $R_E = 200$, $R = 40$, $P_p = 50$ dBm, $P_s = 30$ dBm, $\alpha = 2$, $\gamma_{Th} = 1$, and $\sigma_n^2 = 0.0005$.

For the proposed multiple-ring model, channel effects such as path loss, fading, and shadowing were incorporated while shadowing was not considered for the nearest interferer approximation due to mathematical complexity.

For the multiple-ring model, the number of interfering CR nodes in a particular ring was modeled as a Poisson process, and two fading models were considered; namely, a Rayleigh fading channel, and a composite fading model with the Generalized- K distribution. The exact MGF of the aggregate interference was obtained for both the cases. For the special case of a fixed number (deterministic) of interferer nodes in the rings, the PDF of the aggregate interference was also derived. The exact and asymptotic outage probabilities were derived, and it was shown that the multiple-ring model can be used to accurately approximate the annular underlay model.

In the nearest interferer approximation, the interference from the closest interferer node was approximated to the aggregate interference. The distribution of the distance from the PR to the nearest interferer was derived and analyzed. The ex-

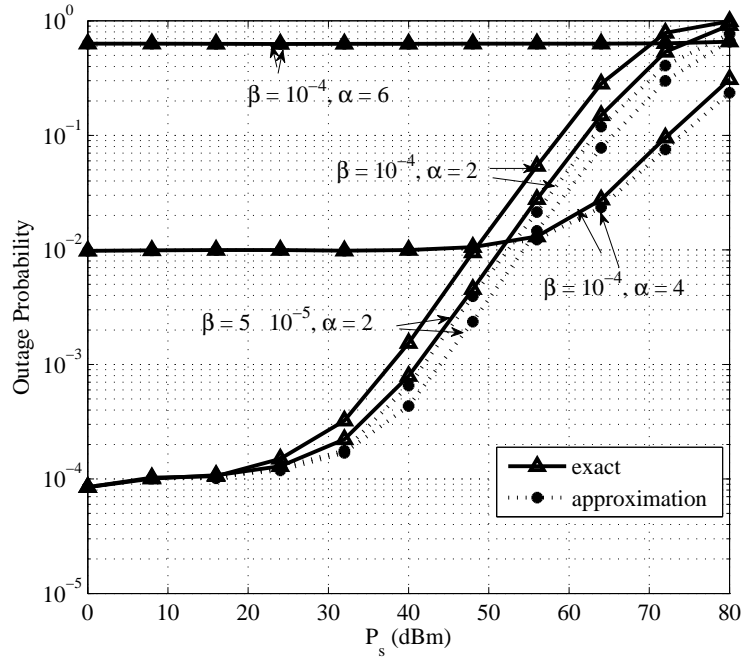


Figure 4.15: Outage probability vs P_s for different values of β and α , with $R_E = 200$, $R_G = 20$, $R = 10$, $P_p = 60$ dBm, $\gamma_{Th} = 1$, and $\sigma_n^2 = 0.001$.

act MGF of the interference for the approximation was derived for two scenarios; namely, when the interferer nodes employ no power control, and when they employ a distance based power control scheme. The outage probability was analyzed using the derived MGFs when the primary signals also undergo Rayleigh fading. Simulations confirmed the analysis and established that the approximation is extremely tight under certain conditions. These conditions are higher path loss exponents, lower node densities, and larger exclusion regions. Furthermore, the transmitter-receiver distance of the primary network has minimal bearing on the accuracy of the approximation.

~

Chapter 5

Conclusions and Future Research Directions

5.1 Conclusions

This thesis investigated the aggregate interference on the primary receiver from a random number of cognitive nodes accessing the licensed spectrum concurrently with the primary system. The annular underlay network of cognitive radio nodes, which was modeled as a Poisson point process, was considered.

Chapter 2 analyzed the aggregate interference under composite Rayleigh fading and Gamma shadowing from interferer nodes in the annular model. The MGF of the aggregate interference, moments, outage, and asymptotic expressions were derived. The variation of outage under different shadowing conditions was lower at high path loss exponent values. Furthermore, the aggregate interference was shown to be reasonably approximated by a Gamma distribution.

In Chapter 3, a new Multiple-ring model for the interference was proposed. The proposed model was shown to be highly versatile and mathematically simple while being extremely accurate. The accuracy vs complexity was shown to be adjustable by varying system parameters. Moreover, the ability of the proposed model to accurately model different systems was discussed. Furthermore, the interference from the nearest interferer node was analyzed. Under certain system conditions, the nearest interferer dominates the aggregate interference, and yields a reasonable

approximation.

5.2 Future Research Directions

Several improvements and extensions can be performed in the future.

- **Secondary medium access control**

The analysis did not consider mutual interference among CR nodes. For example, if a particular CR is receiving, another nearby CR transmission will cause interference. Thus, medium access in the secondary network can be considered for a more realistic analysis.

- **Non-homogeneous cases**

While interferer nodes were assumed to be a homogeneous Poisson process, this may not always be a valid assumption, and non-homogeneous analysis could prove useful. For example, in a city, node density decreases as the distance from the city center increases. Moreover, interferer nodes distributed in clusters can also be considered where the aggregate interference is due to signals from multiple clusters.

- **Mobility of nodes**

The interferer nodes have been assumed to be static. In practice, these nodes can move around randomly. Such mobility leads to time varying interference, and analytical results may be derived for those cases. Moreover, the power level of the interferer nodes has been assumed to be static in most cases. However, due to various dynamic power control schemes and system configurations, the power levels of the different interferer nodes vary in time.

- **Correlated fading/shadowing**

The work has assumed independent fading/shadowing on the links between the different interferer nodes and the primary receiver. A possible extension is to consider correlations in these variables.

- **Analysis of different channel models**

This extension to the work includes carrying out the interference analysis for different fading/shadowing and path loss models.

~

Bibliography

- [1] Qualcomm. (2011) The visible light communications motivation. [Online]. Available: <http://visiblelightcomm.com/the-visible-light-communications-motivation/>
- [2] I. Gradshteyn and I. Ryzhik, *Table of Integrals, Series, and Products*, 7th ed. Academic Press, 2007.
- [3] A. Molisch, *Wireless Communications*. Wiley-IEEE Press, 2011.
- [4] Cisco. (2012) Cisco visual networking index: Global mobile data traffic forecast update: 2011-2016. [Online]. Available: http://www.cisco.com/en/US/solutions/collateral/ns341/ns525/ns537/ns705/ns827/white_paper_c11-520862.html
- [5] ITU. (2012) Key statistical highlights: ITU data release june 2012. [Online]. Available: http://www.itu.int/ITU-D/ict/statistics/material/pdf/2011%20Statistical%20highlights_June_2012.pdf
- [6] S. Haykin, “Cognitive radio: brain-empowered wireless communications,” *IEEE J. Sel. Areas Commun.*, vol. 23, no. 2, pp. 201–220, Feb. 2005.
- [7] J. Mitola, “Cognitive radio: An integrated agent architecture for software defined radio,” Ph.D. dissertation, KTH Royal Inst. of Technol., Stockholm, Sweden, 2000.
- [8] I. F. Akyildiz, W.-Y. Lee, M. C. Vuran, and S. Mohanty, “Next generation/dynamic spectrum access/cognitive radio wireless networks: A survey,” *Computer Networks*, vol. 50, no. 13, pp. 2127–2159,

2006. [Online]. Available: <http://www.sciencedirect.com/science/article/pii/S1389128606001009>
- [9] R. Menon, R. Buehrer, and J. Reed, "Outage probability based comparison of underlay and overlay spectrum sharing techniques," in *Proc. IEEE DYSpan 2005*, Nov. 2005, pp. 101–109.
- [10] B. Wang and K. Liu, "Advances in cognitive radio networks: A survey," *IEEE J. Sel. Topics Signal Process.*, vol. 5, no. 1, pp. 5–23, Feb. 2011.
- [11] S. Srinivasa and S. Jafar, "Cognitive radios for dynamic spectrum access - the throughput potential of cognitive radio: A theoretical perspective," *IEEE Commun. Mag.*, vol. 45, no. 5, pp. 73–79, May 2007.
- [12] E. Hossain, D. Niyato, and Z. Han, *Dynamic Spectrum Access and Management in Cognitive Radio Networks*. Cambridge University Press, 2009.
- [13] M. Vu, S. Ghassemzadeh, and V. Tarokh, "Interference in a cognitive network with beacon," in *Proc. IEEE WCNC 2008*, Apr. 2008, pp. 876–881.
- [14] M. Sherman, A. Mody, R. Martinez, C. Rodriguez, and R. Reddy, "IEEE standards supporting cognitive radio and networks, dynamic spectrum access, and coexistence," *IEEE Commun. Magazine*, vol. 46, no. 7, pp. 72–79, Jul. 2008.
- [15] C. Stevenson, G. Chouinard, Z. Lei, W. Hu, S. Shellhammer, and W. Caldwell, "IEEE 802.22: The first cognitive radio wireless regional area network standard," *IEEE Commun. Magazine*, vol. 47, no. 1, pp. 130–138, Jan. 2009.
- [16] K. Moessner, H. Harada, C. Sun, Y. Alemseged, H. N. Tran, D. Nogueta, R. Sawai, and N. Sato, "Spectrum sensing for cognitive radio systems: technical aspects and standardization activities of the IEEE P1900.6 working group," *IEEE Wireless Commun.*, vol. 18, no. 1, pp. 30–37, Feb. 2011.
- [17] A. Damnjanovic, J. Montojo, Y. Wei, T. Ji, T. Luo, M. Vajapeyam, T. Yoo, O. Song, and D. Malladi, "A survey on 3GPP heterogeneous networks," *IEEE Wireless Commun.*, vol. 18, no. 3, pp. 10–21, 2011.

- [18] R. Research. (2011) Efficient use of spectrum. [Online]. Available: http://www.rysayv.com/Articles/2011_05_Rysavy_Efficient_Use_Spectrum.pdf
- [19] J. Hoydis, M. Kobayashi, and M. Debbah, "Green small-cell networks," *Vehicular Technology Magazine, IEEE*, vol. 6, no. 1, pp. 37–43, 2011.
- [20] A. Goldsmith, *Wireless Communications*. Cambridge University Press, 2005.
- [21] M. Simon and M. S. Alouini, *Digital Communications over Fading Channels, 2nd edition*. Wiley, 2004.
- [22] M. Nakagami, "The m-distribution, a general formula for intensity distribution of rapid fading," *Statistical Methods in RadioWave Propagation*, pp. 3–36, 1960.
- [23] I. Trigui, A. Laourine, S. Affes, and A. Stephenne, "Outage analysis of wireless systems over composite fading/shadowing channels with co-channel interference," in *Proc. IEEE WCNC*, Apr. 2009, pp. 1–6.
- [24] P. Bithas, N. Sagias, P. Mathiopoulos, G. Karagiannidis, and A. Rontogiannis, "On the performance analysis of digital communications over generalized-K fading channels," *IEEE Commun. Lett.*, vol. 10, no. 5, pp. 353–355, May 2006.
- [25] S. Atapattu, C. Tellambura, and H. Jiang, "A mixture gamma distribution to model the SNR of wireless channels," vol. 10, no. 12, pp. 4193–4203, Dec. 2011.
- [26] G. L. Stuber, *Principles of Mobile Communication*. Kluwer Academic Publishers, Norwell, MA, 2001.
- [27] D. Lewinski, "Nonstationary probabilistic target and clutter scattering models," *IEEE J. Antennas and Propagation*, vol. 31, no. 3, pp. 490–498, May 1983.
- [28] I. Kostic, "Analytical approach to performance analysis for channel subject to shadowing and fading," *IEEE Proc. Commun.*, vol. 152, no. 6, pp. 821–827, Dec. 2005.

- [29] S. Al-Ahmadi and H. Yanikomeroglu, "On the approximation of the generalized-K distribution by a gamma distribution for modeling composite fading channels," *IEEE Trans. Wireless Commun.*, vol. 9, no. 2, pp. 706–713, Feb. 2010.
- [30] Z. Chen, C.-X. Wang, X. Hong, J. Thompson, S. Vorobyov, X. Ge, H. Xiao, and F. Zhao, "Aggregate interference modeling in cognitive radio networks with power and contention control," *IEEE Trans. Commun.*, vol. 60, no. 2, pp. 456–468, Feb. 2012.
- [31] N. Hoven and A. Sahai, "Power scaling for cognitive radio," in *Proc. IEEE WNCMC*, vol. 1, 2005, pp. 250–255 vol.1.
- [32] J. F. Kingman, *Poisson Processes*. Oxford University Press, 1993.
- [33] I. Janine, A. Penttinen, H. Stoyan, and D. Stoyan, *Statistical Analysis and Modelling of Spatial Point Patterns (Statistics in Practice)*. Wiley-Interscience, 2008.
- [34] A. Baddeley, I. Barany, R. Schneider, and W. Weil, *Spatial Point Processes and their Applications*. Springer, 2007.
- [35] K. Gulati, B. Evans, J. Andrews, and K. Tinsley, "Statistics of co-channel interference in a field of Poisson and Poisson-Poisson clustered interferers," *IEEE Trans. Signal Process.*, vol. 58, no. 12, pp. 6207–6222, Dec. 2010.
- [36] E. Salbaroli and A. Zanella, "Interference analysis in a Poisson field of nodes of finite area," *IEEE Trans. Veh. Technol.*, vol. 58, no. 4, pp. 1776–1783, May 2009.
- [37] E. Sousa and J. Silvester, "Optimum transmission ranges in a direct-sequence spread-spectrum multihop packet radio network," *IEEE J. Sel. Areas Commun.*, vol. 8, no. 5, pp. 762–771, Jun. 1990.

- [38] E. Sousa, "Performance of a spread spectrum packet radio network link in a Poisson field of interferers," *IEEE Trans. Signal Process.*, vol. 38, no. 6, pp. 1743–1754, Nov. 1992.
- [39] J. Ilow and D. Hatzinakos, "Analytic alpha-stable noise modeling in a Poisson field of interferers or scatterers," *IEEE Trans. Signal Process.*, vol. 46, no. 6, pp. 1601–1611, Jun. 1998.
- [40] P. C. Pinto and M. Z. Win, "Communication in a Poisson field of interferers—part I: Interference distribution and error probability," *IEEE Trans. Wireless Commun.*, vol. 9, no. 7, pp. 2176–2186, Jul. 2010.
- [41] C.-H. Lee and M. Haenggi, "Interference and outage in Poisson cognitive networks," *IEEE Trans. Wireless Commun.*, vol. 11, no. 4, pp. 1392–1401, Apr. 2012.
- [42] R. Ganti and M. Haenggi, "Interference and outage in clustered wireless ad hoc networks," *IEEE Trans. Info. Theory*, vol. 55, no. 9, pp. 4067–4086, 2009.
- [43] G. Alfano, M. Garetto, and E. Leonardi, "Capacity scaling of wireless networks with inhomogeneous node density: upper bounds," *IEEE J. Sel. Areas Commun.*, vol. 27, no. 7, pp. 1147–1157, 2009.
- [44] J. Chen, M. Ding, and Q. Zhang, "Interference statistics and performance analysis of mimo ad hoc networks in binomial fields," *IEEE Trans. Veh. Technol.*, vol. 61, no. 5, pp. 2033–2043, Jun. 2012.
- [45] D. Stoyan, W. S. Kendall, and J. Mecke, *Stochastic Geometry and Its Applications*. Wiley, 1996.
- [46] M. Aljuaid and H. Yanikomeroglu, "A cumulant-based characterization of the aggregate interference power in wireless networks," in *Proc. IEEE VTC, Ottawa, Canada*, May 2010, pp. 1–5.
- [47] M. Timmers, S. Pollin, A. Dejonghe, A. Bahai, L. Van der Perre, and F. Catthoor, "Accumulative interference modeling for cognitive radios with

- distributed channel access,” in *Proc. IEEE CrownCom, Singapore*, May 2008, pp. 1–7.
- [48] S. SINGH, N. Mehta, A. Molisch, and A. Mukhopadhyay, “Moment-matched lognormal modeling of uplink interference with power control and cell selection,” *IEEE Trans. Wireless Commun.*, vol. 9, no. 3, pp. 932–938, Mar. 2010.
- [49] L. Vijayandran, P. Dharmawansa, T. Ekman, and C. Tellambura, “Analysis of aggregate interference and primary system performance in finite area cognitive radio networks,” *IEEE Trans. Commun.*, vol. PP, no. 99, pp. 1–12, 2012.
- [50] A. Ghasemi and E. Sousa, “Interference aggregation in spectrum-sensing cognitive wireless networks,” *IEEE J. Sel. Areas Commun.*, vol. 2, no. 1, pp. 41–56, Feb. 2008.
- [51] T. Velivasaki, T. Zahariadis, P. Trakadas, and C. Capsalis, “Interference analysis of cognitive radio networks in a digital broadcasting spectrum environment,” in *Proc. IEEE IWSSIP*, Jun. 2009, pp. 1–5.
- [52] A. Rabbachin, T. Q. S. Quek, H. Shin, and M. Z. Win, “Cognitive network interference,” *IEEE J. Sel. Areas Commun.*, vol. 29, no. 2, pp. 480–493, Feb. 2011.
- [53] M. Aljuaid and H. Yanikomeroglu, “Investigating the gaussian convergence of the distribution of the aggregate interference power in large wireless networks,” *IEEE Trans. Veh. Technol.*, vol. 59, no. 9, pp. 4418–4424, Nov. 2010.
- [54] M. Vu, N. Devroye, and V. Tarokh, “On the primary exclusive region of cognitive networks,” *IEEE Trans. Wireless Commun.*, vol. 8, no. 7, pp. 3380–3385, Jul. 2009.
- [55] A. Hasan and J. Andrews, “The guard zone in wireless ad hoc networks,” *IEEE Trans. Commun.*, vol. 6, no. 3, pp. 897–906, Mar. 2007.

- [56] M. J. Rahman and X. Wang, "Probabilistic analysis of mutual interference in cognitive radio communications," in *Proc. IEEE GLOBECOM*, Dec. 2011, pp. 1–5.
- [57] M. Derakhshani and T. Le-Ngoc, "Aggregate interference and capacity-outage analysis in a cognitive radio network," *IEEE Trans. Veh. Technol.*, vol. 61, no. 1, pp. 196–207, Jan. 2012.
- [58] M. Hanif, M. Shafi, P. Smith, and P. Dmochowski, "Interference and deployment issues for cognitive radio systems in shadowing environments," in *Proc. IEEE ICC*, Jun. 2009, pp. 1–6.
- [59] A. Babaei and B. Jabbari, "Interference modeling and avoidance in spectrum underlay cognitive wireless networks," in *Proc. IEEE ICC*, May 2010, pp. 1–5.
- [60] K. Woyach, P. Grover, and A. Sahai, "Near vs. far field: Interference aggregation in tv whitespaces," in *Proc. IEEE GLOBECOM*, Dec. 2011, pp. 1–5.
- [61] X. Hong, C.-X. Wang, and J. Thompson, "Interference modeling of cognitive radio networks," in *Proc. IEEE VTC*, May 2008, pp. 1851–1855.
- [62] P. G. Moschopoulos, "The distribution of the sum of independent gamma random variables," *Ann. Inst. Statist. Math.*, vol. 37, pp. 541–544, 1985.
- [63] D. Wackerly and W. Scheaffer, *Mathematical Statistics with Applications*. Thomson Higher Education, 2008.
- [64] V. Mordachev and S. Loyka, "On node density - outage probability tradeoff in wireless networks," *IEEE J. Sel. Areas Commun.*, vol. 27, no. 7, pp. 1120–1131, 2009.
- [65] Y. Wen, S. Loyka, and A. Yongacoglu, "The impact of fading on the outage probability in cognitive radio networks," in *Proc. IEEE VTC 2010-Fall*, Sep. 2010, pp. 1–5.

- [66] M. Hoyhtya and A. Mammela, “Adaptive inverse power control using an FxLMS algorithm,” in *Proc. IEEE VTC*, Apr. 2007, pp. 3021–3025.